One-step Reprogramming of Human Fibroblasts into Oligodendrocyte-like Cells by SOX10, OLIG2, and NKX6.2

Konstantina Chanoumidou, Benjamín Hernández-Rodríguez, Farina Windener, Christian Thomas, Martin Stehling, Sabah Mozafari, Stefanie Albrecht, Linda Ottoboni, Jack Antel, Kee-Pyo Kim, et al.

Please cite this article in press as: Chanoumidou et al., One-step Reprogramming of Human Fibroblasts into Oligodendrocyte-like Cells by SOX10, OLIG2, and NKX6.2, Stem Cell Reports (2021), https://doi.org/10.1016/j.stemcr.2021.03.001

Stem Cell Reports
Article
ISSCR
OPEN ACCESS

One-step Reprogramming of Human Fibroblasts into Oligodendrocyte-like Cells by SOX10, OLIG2, and NKX6.2

Konstantina Chanoumidou,[1] Benjamín Hernández-Rodríguez,[2] Farina Windener,[1] Christian Thomas,[1] Martin Stehling,[2] Sabah Mozafari,[3,4,5,6] Stefanie Albrecht,[1] Linda Ottoboni,[8] Jack Antel,[7] Kee-Pyo Kim,[2] Sergiy Velychko,[2] Qiao Ling Cui,[7] Yu Kang T. Xu,[12] Gianvito Martino,[8] Jürgen Winkler,[9] Hans R. Schöler,[2,14] Anne Baron-Van Evercooren,[3,4,5,6] Odile Boespflug-Tanguy,[10,11] Juan M. Vaquerizas,[2,13] Marc Ehrlich,[1] and Tanja Kuhlmann[1,*]

[1]Institute of Neuropathology, University Hospital Münster, Pottkamp 2, 48149 Münster, Germany
[2]Max Planck Institute for Molecular Biomedicine, 48149 Münster, Germany
[3]INSERM, U1127, 75013 Paris, France
[4]CNRS, UMR 7225, 75013 Paris, France
[5]Sorbonne Universités UPMC Paris 06, UM-75, 75005 Paris, France
[6]ICM-GH Pitié-Salpêtrière, 75013 Paris, France
[7]Montreal Neurological Institute, McGill University, Montreal, Quebec, Canada
[8]Neuroimmunology Unit, IRCCS San Raffaele Hospital and Vita Salute San Raffaele University, Milan, Italy
[9]Department of Molecular Neurology, University Hospital Erlangen, Friedrich-Alexander-Universität Erlangen- Nürnberg, Schwabachanlage 6, 91054 Erlangen, Germany
[10]Service de Neuropédiatrie et des Maladies Métaboliques, LEUKOFRANCE, AP-HP, Hôpital Robert Debré, 75019 Paris, France
[11]Université de Paris, UMR1141 NeuroDiderot, INSERM, 75019 Paris, France
[12]The Solomon H. Snyder Department of Neuroscience, Johns Hopkins University School of Medicine, Baltimore, MD 21205, USA
[13]Medical Research Council London Institute of Medical Sciences, Institute of Clinical Sciences, Faculty of Medicine, Imperial College London, London, UK
[14]University of Münster, Medical Faculty, Domagkstrasse 3, Münster 48149, Germany
*Correspondence: tanja.kuhlmann@ukmuenster.de
https://doi.org/10.1016/j.stemcr.2021.03.001

SUMMARY

Limited access to human oligodendrocytes impairs better understanding of oligodendrocyte pathology in myelin diseases. Here, we describe a method to robustly convert human fibroblasts directly into oligodendrocyte-like cells (dc-hiOLs), which allows evaluation of remyelination-promoting compounds and disease modeling. Ectopic expression of SOX10, OLIG2, and NKX6.2 in human fibroblasts results in rapid generation of $O4^+$ cells, which further differentiate into MBP^+ mature oligodendrocyte-like cells within 16 days. dc-hiOLs undergo chromatin remodeling to express oligodendrocyte markers, ensheath axons, and nanofibers *in vitro*, respond to promyelination compound treatment, and recapitulate *in vitro* oligodendroglial pathologies associated with Pelizaeus-Merzbacher leukodystrophy related to *PLP1* mutations. Furthermore, DNA methylome analysis provides evidence that the CpG methylation pattern significantly differs between dc-hiOLs derived from fibroblasts of young and old donors, indicating the maintenance of the source cells' "age." In summary, dc-hiOLs represent a reproducible technology that could contribute to personalized medicine in the field of myelin diseases.

INTRODUCTION

Oligodendrocytes (OLs), the myelinating cells of the central nervous system (CNS), form and maintain the myelin sheath. Contribution of OLs to axon potential propagation, and trophic and metabolic support of neurons underlines their multifunctional role in CNS and implicates OL dysfunctionality and myelin loss in a wide range of CNS diseases including leukodystrophies, inflammatory demyelinating, neurodegenerative, and psychiatric diseases as well as ischemic or traumatic insults (Franklin and Ffrench-Constant, 2017; Micu et al., 2018; Stangel et al., 2017).

In dys- and demyelinating diseases the myelin sheath is either not properly formed or destroyed (Van Der Knaap and Bugiani, 2017). Promotion of (re-)myelination is a promising treatment strategy; however, the development of new therapeutic methods is hampered by the limited availability of primary human oligodendrocytes. In the past few years, a number of protocols have been developed to generate myelinating oligodendrocytes from human induced pluripotent stem cells (iPSC) in two- and three-dimensional (3D) culture systems (Douvaras and Fossati, 2015; Garcia-Leon et al., 2018; Madhavan et al., 2018). We have recently shown that forced expression of the transcription factors SOX10, OLIG2, and NKX6.2 (SON) significantly accelerates the generation of human stem cell-derived oligodendrocytes and increases the differentiation efficiency in comparison with previous methods (Ehrlich et al., 2017). However, the time-consuming process of somatic cell reprogramming and re-differentiation combined with the high cost and the genetic instability of iPSCs remain obstacles in their clinical application and highlight the need for additional

Please cite this article in press as: Chanoumidou et al., One-step Reprogramming of Human Fibroblasts into Oligodendrocyte-like Cells by SOX10, OLIG2, and NKX6.2, Stem Cell Reports (2021), https://doi.org/10.1016/j.stemcr.2021.03.001

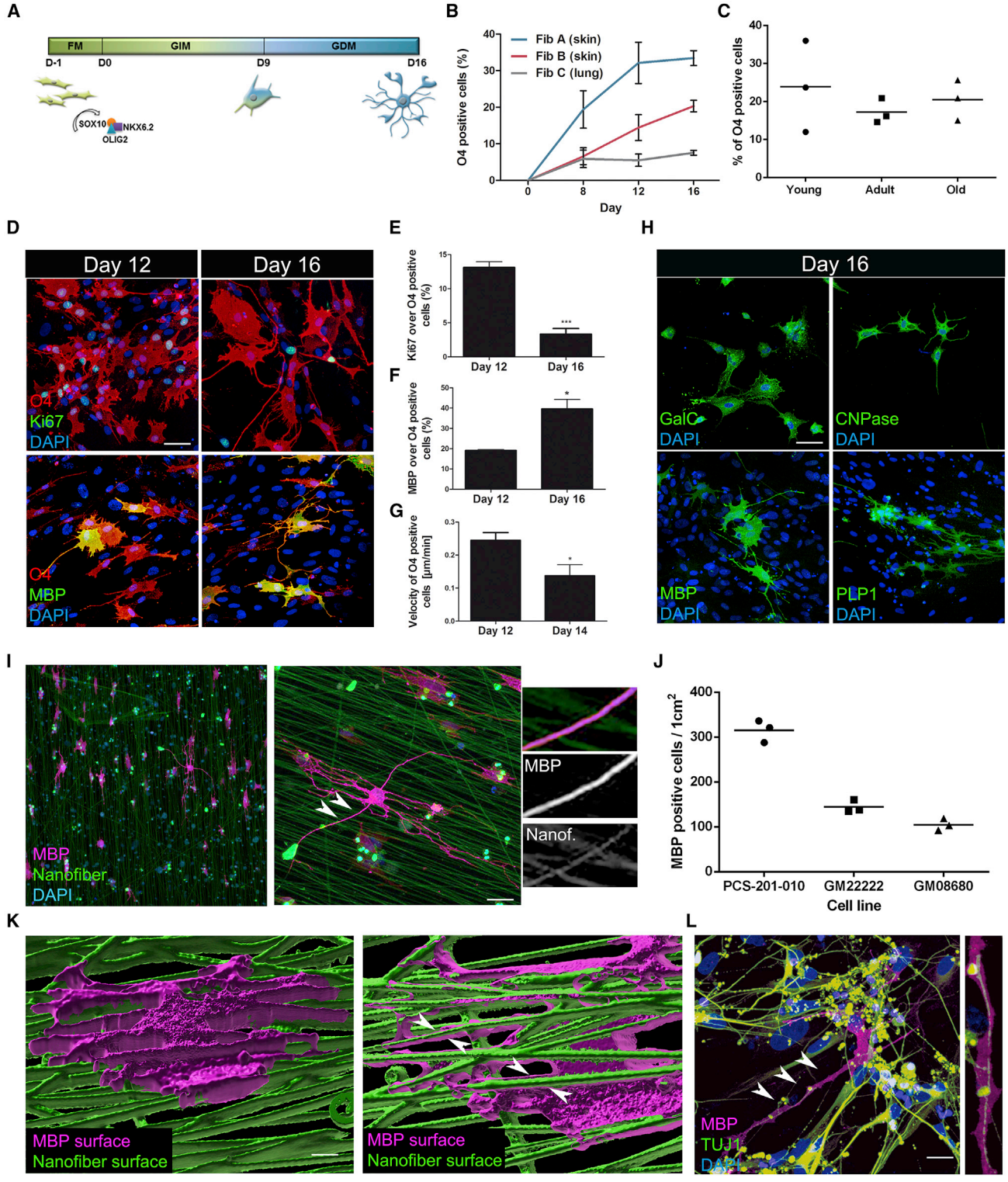

Figure 1. Characterization of dc-hiOLs

(A) Schematic representation of dc-hiOL generation. Fibroblasts are infected with SON lentivirus at day −1 in fibroblast medium (FM). Cells are cultured in glia induction medium (GIM) from day 0 to day 9, after which the medium is switched to glia differentiation medium (GDM) to promote terminal differentiation of oligodendrocyte-like cells.

(legend continued on next page)

experimental models. A limited number of studies have presented transdifferentiation of murine embryonic fibroblasts into oligodendrocytes using different combinations of transcription factors (Matjusaitis et al., 2019; Najm et al., 2013; Yang et al., 2013). Very recently, Pouya et al. (2020) reported direct conversion of human oligodendrocytes but with limited characterization of the induced cells.

Here, we present a robust and highly reproducible protocol for direct conversion of human fibroblasts into oligodendrocyte-like cells. We found that overexpression of SOX10, OLIG2, and NKX6.2, previously shown adequately to differentiate iPSC-derived neural progenitor cells (NPCs) to OLs, is also sufficient to directly reprogram young, adult, and old-aged fibroblasts to directly converted human induced oligodendrocyte-like cells (dc-hiOLs) within 16 days. dc-hiOLs undergo chromatin remodeling to induce key oligodendrocyte markers, display ensheathment capacity *in vitro*, respond to promyelination compound treatment, and recapitulate oligodendroglial pathologies associated with Pelizaeus-Merzbacher leukodystrophy due to *PLP1* mutation. Additionally, DNA methylation profiling indicates that dc-hiOLs retain the epigenetic age signature of donor cells. The technique described here significantly facilitates and advances compound screening and disease-modeling studies as well as the possibility of personalized medicine in the field of dys- and demyelinating diseases.

RESULTS

Overexpression of SOX10, OLIG2, and NKX6.2 Directly Reprograms Human Fibroblasts into Oligodendrocyte-like Cells

To develop a time- and cost-efficient method to generate human oligodendrocytes, we aimed to establish a transdifferentiation approach. Based on our previous observation that ectopic expression of SON in human iPSC-derived NPCs promotes their differentiation into oligodendrocytes, we reasoned that the same factors may directly convert fibroblasts into oligodendrocytes (Ehrlich et al., 2017). Overexpression of SON using a polycistronic lentiviral vector in three different human fetal/newborn fibroblast lines of diverse tissue origin (skin and lung) (Fib A, Fib B, Fib C) resulted in morphological changes as early as 9 days post infection. The cells lost their typical fibroblast spindle-like morphology and acquired a rounder shape followed by progressive extension of branches upon medium enrichment with differentiation factors including NT3, insulin-like growth factor 1 (IGF-1), and dibutyryl cyclic AMP (dbcAMP) for 7 days (Figures 1A and S1A). To further characterize the identity of the cells, we performed flow-cytometry and immunocytochemistry (ICC) analyses using the immature oligodendroglial marker O4. O4$^+$ dc-hiOLs were already detected by post-infection day 8 (Figure 1B). Their percentage increased progressively until day 16, reaching an average conversion efficiency of

(B) Quantification of O4$^+$ cells using flow-cytometry analysis at different time points during the transdifferentiation process for three fetal/neonatal fibroblast cell lines (Fib A, Fib B, and Fib C). Data are shown as the mean ± SEM of n = 4 different transdifferentiation experiments for each cell line.
(C) Comparison of donor cell age effect on transdifferentiation efficiency. Quantification of O4$^+$ cells by fluorescence-activated cell-sorting analysis at day 16. Data are presented as mean of n = 3 different cell lines for fibroblasts from neonatal (newborn to 5 months of age), adult (25–32 years of age), and older (66–71 years of age) donors.
(D) Immunostaining of dc-hiOLs for O4 (red)/Ki67 (green) and O4 (red)/MBP (green) at days 12 and 16 post infection. Scale bar, 50 μm.
(E) Quantification of Ki67$^+$ over O4$^+$ cells at days 12 and 16 of transdifferentiation. Data are presented as the mean + SEM of n = 4 different transdifferentiation experiments of one cell line. Unpaired Student's t test was performed for statistical analysis.
(F) Quantification of MBP$^+$ over O4$^+$ cells at days 12 and 16. Data are presented as the mean + SEM of n = 4 different transdifferentiation experiments of one cell line. Unpaired Student's t test was performed for statistical analysis.
(G) Migration assay using live cell imaging. Graph showing the velocity of purified O4$^+$ cells at days 12 and 14 of direct conversion. Data are presented as the mean + SEM of n = 3 different transdifferentiation experiments of one cell line. Unpaired Student's t test was performed for statistical analysis.
(H) Immunostaining of purified O4$^+$ dc-hiOLs for GalC, CNPase, MBP, and PLP1 (green) at day 16. Scale bar, 50 μm.
(I) Low- and high-magnification confocal images of dc-hiOLs cultured on nanofibers. O4$^+$ cells were purified at day 11 and cultured on FITC-labeled nanofibers for 10 days. Immunostaining of dc-hiOLs for MBP (magenta) shows the alignment of oligodendrocyte processes along the nanofibers (green). Scale bar, 100 μm.
(J) Quantification of MBP$^+$ dc-hiOLs aligned to nanofibers generated from three different cell lines. Three inserts were counted per cell line.
(K) Three-dimensional reconstruction of confocal image of dc-hiOLs stained for MBP (magenta) on FITC-labeled nanofibers illustrates the ensheathment of nanofibers by dc-hiOLs. The clipped view on the rendered surfaces enables one to follow individual nanofibers covered by dc-hiOLs (arrows). Scale bar, 5 μm.
(L) Confocal image of dc-hiOLs co-cultured with iPSC-derived neurons for 6 days. The image illustrates the colocalization of MBP$^+$ (magenta) oligodendrocyte process with neuronal process visualized by TUJ1 (green). Scale bar, 25 μm.
*p < 0.05, ***p < 0.001. See also Figures S1 and S2.

Please cite this article in press as: Chanoumidou et al., One-step Reprogramming of Human Fibroblasts into Oligodendrocyte-like Cells by SOX10, OLIG2, and NKX6.2, Stem Cell Reports (2021), https://doi.org/10.1016/j.stemcr.2021.03.001

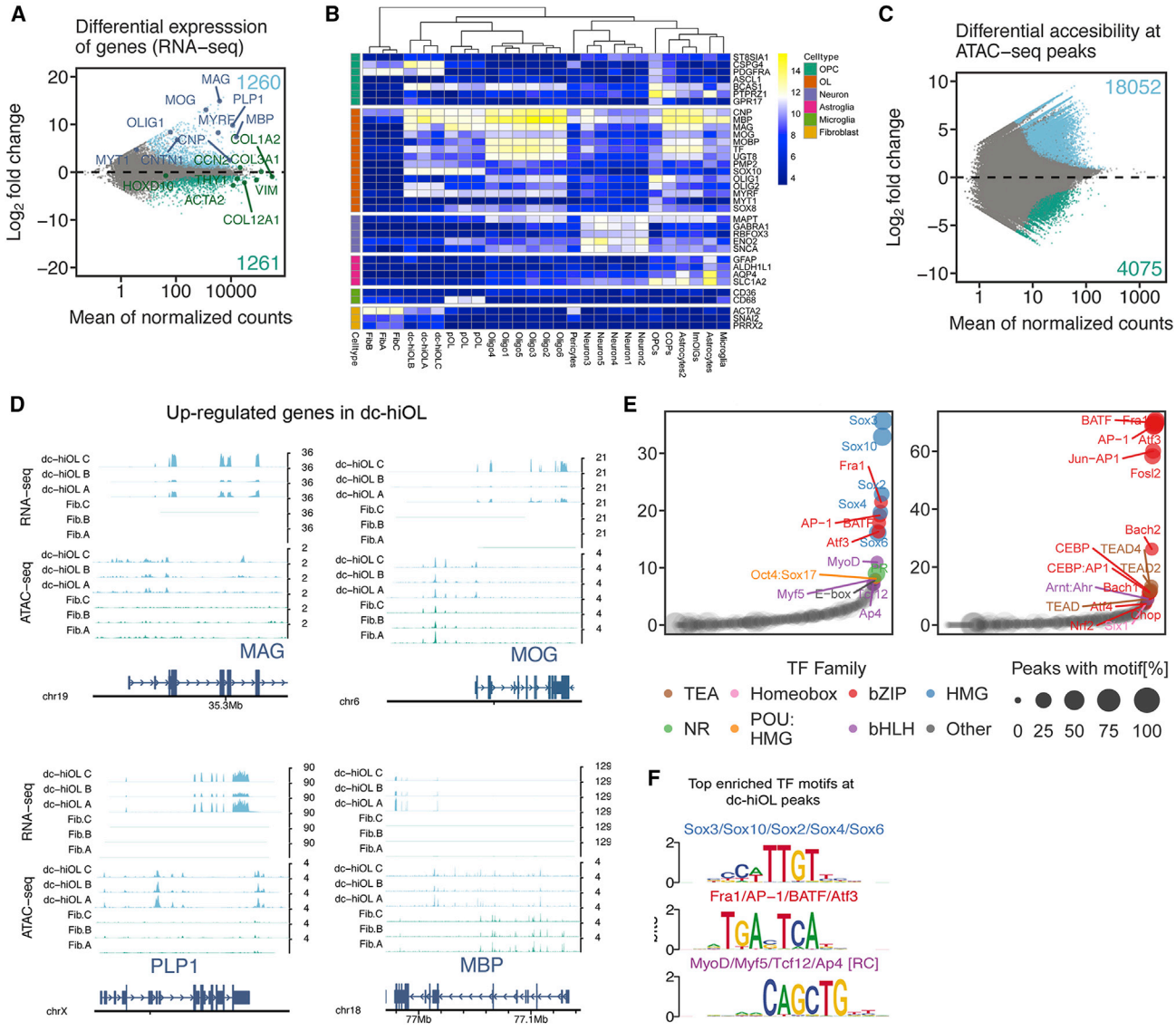

Figure 2. SON Induce Chromatin Remodeling to Activate the Expression of Oligodendrocyte Genes

(A) Global transcriptome comparison using RNA-seq. MA plot comparing gene expression values between dc-hiOLs and fibroblasts. Differentially expressed genes accounting for donor heterogeneity with FDR < 0.01 are color coded. Light-blue dots, dc-hiOL-upregulated genes (1,410); light-green dots, fibroblast-upregulated genes (1,418); dark-blue dots, representative oligodendrocyte marker genes; dark-green dots, representative fibroblast marker genes.

(B) Normalized gene expression values of typical oligodendrocyte progenitor cell (OPC), oligodendrocyte (OL), neuronal, astrocyte, microglia, and fibroblast genes in comparison with single-nuclei RNA-seq data from Jäkel et al. (2019). Fibroblasts (FibA–FibC), induced oligodendrocyte-like cells (dc-hiOLA–dc-hiOLC), and primary human oligodendrocytes (pOl1–pOL3) indicate samples of the present studies. Data from Jäkel et al. (2019) include different subclusters of neurons (Neuron1–Neuron5) and oligodendrocytes (Oligo1–Oligo6), and additional clusters of OPCs, committed OL precursors (COPs), immune oligodendroglia (imOLG), astrocytes (Astrocytes), pericytes (Pericytes), and immune cells (Macrophages and Microglia_Macrophages). Unsupervised hierarchical clustering shows that dc-hiOL1–3 cluster with the other oligodendroglial clusters, whereas fibroblasts (Fib1–Fib3) form a separate cluster. Unexpectedly, in the dataset published by Jäkel et al. (2019), MBP was expressed in comparable levels in oligodendrocytes and astrocytes. This finding might be an RNA-seq artifact.

(C) Global chromatin accessibility comparison using ATAC-seq. MA plot comparing accessibility at ATAC-seq peaks between dc-hiOLs and fibroblasts. Blue dots, peaks preferentially accessible in dc-hiOLs (18,052); light-green dots, fibroblast-accessible peaks (4,075).

(legend continued on next page)

20.4% ± 11.3% and yield of 39.1% ± 13.6% (Figures 1B and S1B–S1D). Control fibroblast cultures infected with the backbone lentiviral vector without SON showed no morphological changes and did not generate any $O4^+$ cells (Figure S1C). Noteworthy, we assessed the reproducibility of the protocol using additional fibroblast samples of various age groups and found no significant effect of donor cell age on the transdifferentiation efficiency (Figure 1C). We followed the kinetics of transdifferentiation by using double-staining for O4 and the cell-cycle marker Ki67 as well as myelin basic protein (MBP), a marker specific for mature oligodendrocytes. Between days 12 and 16 the population of proliferating $O4^+$ cells reduced by 3-fold, whereas the number of $MBP^+/O4^+$ double-positive cells significantly increased, indicating downregulation of proliferation and rapid maturation of dc-hiOLs (Figures 1D–1F). In agreement, live imaging revealed decreased migratory velocity of $O4^+$ cells over time (Figure 1G; Videos S1 and S2). By day 16, besides MBP, dc-hiOLs expressed additional mature oligodendrocyte markers including CNP, GALC, and PLP1 (Figure 1H). Almost no NPCs, neurons, or astrocytes were found using ICC for Nestin, TUJ1, and GFAP, demonstrating the specific transdifferentiation into the oligodendroglial lineage (Figure S1E).

dc-hiOLs Are Stable after Transgene Silencing and Exhibit Ensheathment Capacity *In Vitro*

To test the dependence of dc-hiOLs on transgene expression, we used an SON-internal ribosomal entry site (IRES)-red fluorescent protein (RFP) plasmid for lentiviral transduction of fibroblasts. By day 16, 28.6% of the cells expressed O4 but no longer RFP, demonstrating the maintenance of the oligodendroglial identity after transgene silencing (Figure S1F). Moreover, in support of oligodendroglial fate stability, we observed an upregulated expression of endogenous *SOX10* and *OLIG2* transcripts in cells with silenced transgenes (Figure S1G). Of note, when comparing the expression levels of endogenous *SOX10* and *OLIG2* in fibroblast derived dc-hiOLs and NPC-derived hiOLs, we observed higher expression of both genes in hiOLs. This finding may be attributed to significant expression levels of *SOX10* and *OLIG2* already in NPCs (Figure S1H).

We next analyzed the functional characteristics of the cells by performing *in vitro* myelination assays. $O4^+$ dc-hiOLs were sorted at day 11 post transduction and replated on fluorescein isothiocyanate (FITC)-labeled nanofibers that mimic the structure of neuronal axons or directly on iPSC-derived neurons. After 10 days of culture with nanofibers, dc-hiOLs proceeded to terminal differentiation and exhibited marked morphological change by forming complex MBP^+ processes aligning along (Figures 1I and 1J) and wrapping around nanofibers, as showcased by 3D reconstruction analysis (Figures 1K and S2A). Comparison of dc-hiOLs with iPSC-derived oligodendrocytes co-cultured with nanofibers revealed comparable morphology although with fewer but longer processes (Figures S2B–S2E). Consistently, co-culture of purified $O4^+$ dc-hiOLs with human iPSC-derived neurons already revealed dc-hiOL capacity to recognize and ensheath neuronal processes after 6 days of co-culture (Figure 1L).

Fibroblasts Undergo Changes in Chromatin Accessibility to Induce the Oligodendrocyte-Related Transcriptional Program

To further characterize the induced cells, we analyzed the global gene expression profile of $O4^+$ dc-hiOLs purified at day 16. The transcriptome of dc-hiOLs was analyzed by RNA sequencing (RNA-seq) and compared with that of the original fibroblasts and adult primary human oligodendrocytes from three non-related individuals. Pairwise differential gene expression analysis showed a clear upregulation of the oligodendrocyte transcriptional program as showcased by the high expression of key oligodendrocyte marker genes such as *MOG*, *MAG*, *PLP1*, and *OLIG1* (Figure 2A). Importantly, this is comparable with that of primary human oligodendrocytes (Figure S3A). Unsupervised hierarchical clustering (Figure S3B) confirmed a high similarity of biological replicates within the same cell type (minimum replicate correlation coefficient $\rho = 0.89$) and showed an increased similarity between the signature of dc-hiOLs and primary oligodendrocytes compared with fibroblasts. The expression signature of dc-hiOL clusters together with that of its progenitor fibroblasts suggested a partially preserved fibroblast identity. However, gene

(D) Example of oligodendroglial markers genes upregulated upon SON overexpression. Upper half: normalized RNA-seq coverage across donors (reads per kilobase per million [RPKM]). Lower half: normalized ATAC-seq accessible fraction coverage across donors (RPKM). Blue tracks, dc-hiOL signal; green tracks, fibroblast signal. Coordinates: 'chr19:35,289,212-35,305,038' (MAG), 'chr6:29,642,061-29,674,746' (MOG), 'chr18:76,970,725-77,144,324' (MBP), 'chrX:103,772,927-103,797,741' (PLP1).

(E) Ranked TF motif enrichment within top ATAC-seq peaks as assessed by HOMER (Heinz et al., 2010). Motifs with FDR < 0.05 are color coded. Circle color denotes TF family and circle size the percentage of peaks containing the motif. Inset trees quantify the similarity between obtained motifs (hierarchical clustering using Euclidean distance; bar indicates Euclidean distance of 1). Similar motifs (Pearson correlation coefficient >0.75) were merged into ensemble motifs. Original motifs are presented in Figure S3H.

(F) Top three non-redundant enriched motifs at dc-hiOL accessible peaks.

See also Figure S3.

Please cite this article in press as: Chanoumidou et al., One-step Reprogramming of Human Fibroblasts into Oligodendrocyte-like Cells by SOX10, OLIG2, and NKX6.2, Stem Cell Reports (2021), https://doi.org/10.1016/j.stemcr.2021.03.001

ontology and pathway annotations showed a dc-hiOL-specific enrichment for genes known to be involved in oligodendrocyte differentiation, myelination, and nervous system processes (Figure S3C). Up- and downregulation of representative oligodendroglial and fibroblast-specific genes was confirmed by qPCR analysis (Figures S3D and S3E). Importantly, we compared our RNA-seq data of dc-hiOLs and primary oligodendrocytes (pOls) with a previously published single-nuclei RNA-seq dataset from white matter areas of human brain (Jäkel et al., 2019). When comparing the expression levels of representative glial, neuronal, and fibroblast genes, dc-hiOLs clustered together with primary pOls as well as oligodendrocytes and oligodendrocyte progenitor cells isolated from human brain samples and were clearly separated from fibroblasts (Figure 2B).

We next utilized an assay for transposase-accessible chromatin using sequencing (ATAC-seq) to interrogate changes in chromatin accessibility induced by SON. During transdifferentiation the cells undergo marked chromatin rearrangement as denoted by the analysis of differentially accessible ATAC-seq peaks between fibroblasts and the derived dc-hiOLs (Figures 2C and S3F). Higher incidence of ATAC-seq peaks were identified in promoter and intronic regions (Figure S3G). Distribution of peaks of open chromatin regions were identified within the regulatory regions in core oligodendrocyte markers concomitantly with their increased expression in dc-hiOLs (Figure 2D). To gain more insights into the mechanism of reprogramming, we analyzed transcription factor (TF) binding sites (false discovery rate [FDR] < 0.05) within the open chromatin regions. Among the top enriched TF motifs in dc-hiOLs were several members of the SOX family that are crucial for oligodendroglial cell fate and/or regulation of oligodendroglial differentiation, such as SOX2 and SOX3 (Hoffmann et al., 2014) (Figures 2E and 2F). Only few of the top enriched TF motifs detected in fibroblasts were still among the top enriched TF motifs in dc-hiOLs (Figure S3H).

Test of Promyelination Compounds on dc-hiOLs

Promotion of endogenous remyelination is a key target for therapeutic intervention in multiple sclerosis, dysmyelinating disorders, and CNS injury. iPSC-derived oligodendrocytes have been successfully used as a tool to test compounds (Ehrlich et al., 2017; Garcia-Leon et al., 2018). To determine whether dc-hiOLs can serve as an alternative and faster system for the evaluation of remyelination-promoting compounds, we tested the effect of benztropine, clemastine, and miconazole on dc-hiOLs. All tested compounds have been previously shown to promote oligodendroglial differentiation *in vitro* and *in vivo* (Deshmukh et al., 2013; Ehrlich et al., 2017; Garcia-Leon et al., 2018; Najm et al., 2015).

Starting at day 5 of the protocol, cultures were treated with 1 μM of the aforementioned compounds for 11 days (Figure 3A). Vehicle (DMSO) and T3 treatment were used as negative and positive control, respectively, and assay validation was performed by immunostaining for O4 and MBP. None of the compounds had a positive effect on the number of immature $O4^+$ cells (Figures 3B and 3C). Benztropine and clemastine enhanced the terminal differentiation and maturation of dc-hiOLs to MBP^+ OLs to a similar extent as T3, while miconazole showed a milder but still significant effect (Figures 3B and 3D). These findings suggest that dc-hiOLs can serve as a suitable system for rapid testing of promyelination candidates.

dc-hiOLs Derived from PMD Patients Exhibit Disease-Related Features

We then sought to test whether directly converted OLs from patients with leukodystrophies display pathogenic phenotypes enabling *in vitro* disease modeling. We focused on Pelizaeus-Merzbacher disease (PMD), a rare monogenic disorder caused by distinct types of *PLP1* mutations that is characterized by dysmyelination and broad clinical severity. To assess whether dc-hiOLs can recapitulate the phenotypic heterogeneity of PMD, we analyzed the pathology of OLs derived from a patient with a severe PMD (form 0) related to a *PLP1* missense mutation (cPLP1 643C>T, p.Pro215Ser) as well as from three patients with intermediate forms of PMD (form 2) related to *PLP1* duplication (PLP1 dupl.). Diseased cells were compared with sex- and age-matched controls. As demonstrated by the quantification of $O4^+$ and MBP^+ cells, PLP1 643C>T dc-hiOLs, but not PLP1 dupl., was associated with impaired terminal differentiation to MBP-expressing cells (Figures 4A–4D, S4A, and S4B). Previous works associated defective myelination of OLs with point mutations in *PLP1* with ER stress and vulnerability to cell death (Nevin et al., 2017; Numasawa-Kuroiwa et al., 2014). Accordingly, immunostaining for PLP1 and apoptosis assay at day 13 showed strong perinuclear accumulation of PLP1, indicative of ER stress, and significantly higher number of PLP1 643C>T dc-hiOLs with active caspase-3/7 compared with control cells, respectively (Figures 4E–4G). On the contrary, PLP1 dupl. led to a milder phenotype with preserved PLP1 expression throughout the cytoplasm accompanied by rather perinuclear accumulation and moderately increased level of caspase activity (Figures 4B and S4C). Due to the stronger effect of the *PLP1* point mutation, we further studied PLP1 643C>T dc-hiOLs and tried to reverse the pathogenic phenotype. Cell treatment with GSK2656157, a PERK inhibitor, rescued caspase activity (Figure 4G) and terminal differentiation to MBP-expressing cells (Figure 4H) denoting ER stress involvement in the pathogenesis of PLP1 643C>T mutation, as described earlier (Numasawa-Kuroiwa et al., 2014).

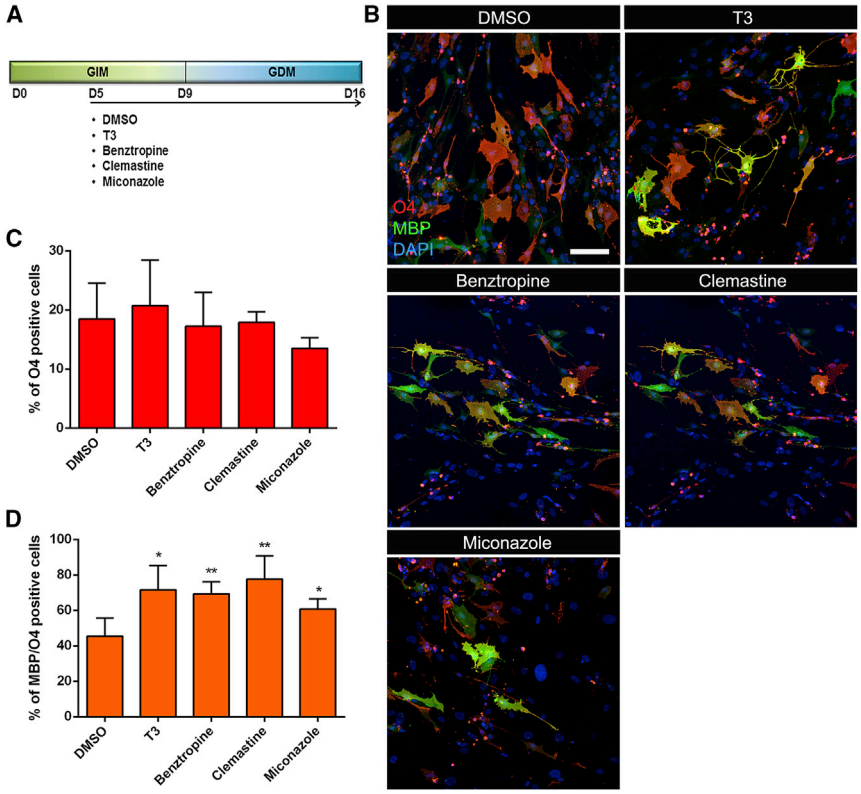

Figure 3. dc-hiOLs Respond to Promyelination Compound Treatment

(A) Schematic representation of the promyelination drug test on dc-hiOLs. Cells were treated with DMSO, T3, benztropine (1 μM), clemastine (1 μM), or miconazole (1 μM) from day 5 to day 16 of transdifferentiation.

(B) ICC for MBP (green) and O4 (red) at day 16. Scale bar: 50 μm.

(C and D) Quantification of $O4^+$/DAPI (C) and $MBP^+/O4^+$ (D) cells at day 16. Counting of positive cells was performed manually by analyzing ten fields captured randomly using 20× magnification for each condition in all tested cell lines. Data are shown as the mean + SEM of four different cell lines (n = 4). Significance was determined by two-tailed unpaired t test. *p < 0.05, **p < 0.01.

dc-hiOLs Maintain the Epigenetic Age of Donor Cells

A fundamental challenge in using reprogrammed cells to study age-related traits is the preservation of donor cells' "age." While iPSC reprogramming is accompanied by cell rejuvenation and erasure of aging signature (Lapasset et al., 2011; Meissner et al., 2008), directly converted cells maintain many features of aging (Huh et al., 2016; Mertens et al., 2015). The strong correlation between cellular age and DNA methylation (Fraga and Esteller, 2007) prompted us to study whether dc-hiOLs retain the epigenetic age signature of their cells of origin.

DNA methylation patterns of dc-hiOLs and corresponding fibroblasts were analyzed across three donor age groups: neonatal (between newborn and 5 months of age), adult (between 25 and 32 years of age), and old age (between 66 and 71 years of age). We first analyzed differentially methylated CpG sites in key oligodendrocyte genes. Comparing methylation β values between dc-hiOLs and fibroblasts shows significant hypomethylation of CpGs mapping to *MBP*, whereas there were no differences in methylation levels of *MAG* and *MOG* (Figure 5A) although they are highly expressed in dc-hiOLs, suggesting additional transcriptional regulatory mechanisms. Unsupervised analysis of differentially methylated regions between dc-hiOL and fibroblast samples confirmed a significantly hypomethylated region of 17 CpG sites mapping to exon 1 of MBP transcripts typically expressed in the brain (Figure 5B, HMM-Fisher, $p = 1 \times 10^{-19}$). We observed a high epigenetic divergence of adult/old samples as compared with neonatal samples (adult/old versus neonatal: 57,106 differentially methylated CpG sites, adjusted $p < 0.05$). Analysis of the top 10,000 most variable CpG sites of all 57,106 age-associated CpGs showed that the age signature of dc-hiOLs is maintained throughout transdifferentiation and reflects the age of donor cells (Figure 5C). Cells from adult and old-aged donors rather display global DNA methylation patterns similar to those shown on unsupervised t-distributed stochastic neighbor embedding (t-SNE) analysis (Figure 4D), indicating that age-related epigenetic changes take already place in early adulthood. Gene ontology term analysis of the differentially methylated CpGs between neonatal and adult/old-aged samples revealed many developmental annotations as well as other processes associated with transcriptional regulation and post-translational modifications (Table S1). In line with t-SNE dimensionality reduction, unsupervised hierarchical clustering of the top 5.000 most variable CpGs clearly separated neonatal samples from dc-hiOLs derived from adult and old-aged donors (Figure S5A). We applied Horvath's epigenetic clock (Horvath, 2013) as age predictor to our

Please cite this article in press as: Chanoumidou et al., One-step Reprogramming of Human Fibroblasts into Oligodendrocyte-like Cells by SOX10, OLIG2, and NKX6.2, Stem Cell Reports (2021), https://doi.org/10.1016/j.stemcr.2021.03.001

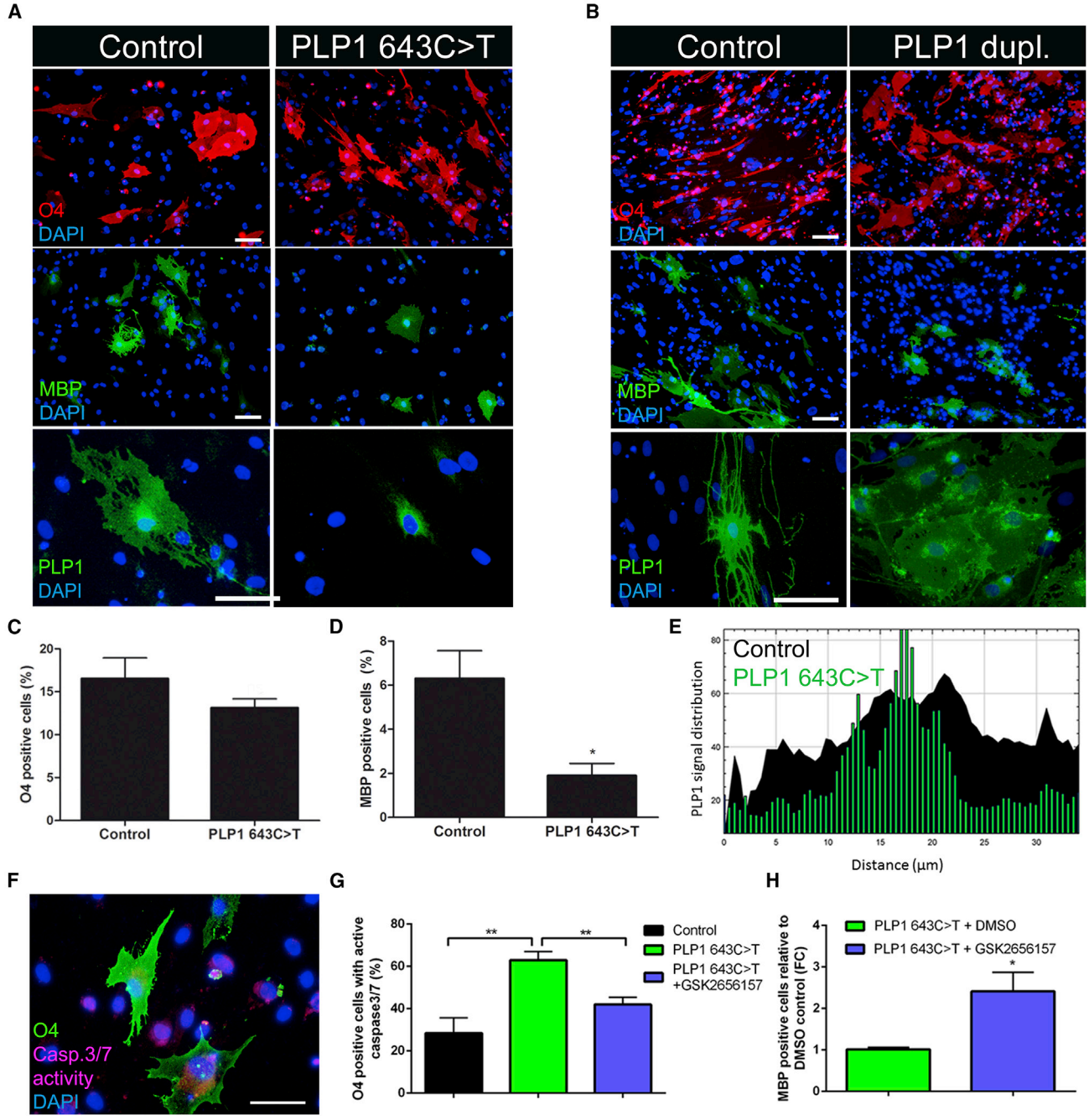

Figure 4. dc-hiOLs Derived from PMD Patients Recapitulate Disease-Related Pathologies

Characterization of dc-hiOLs derived from PMD patients. dc-hiOLs derived from one PMD patient with a point mutation (PLP1 643C>T) and three PMD patients with *PLP1* duplication (PLP1 dupl.) were compared with sex- and aged-matched healthy controls, respectively.

(A and B) Representative immunofluorescence images of $O4^+$ (red), MBP^+ (green), and $PLP1^+$ (green) dc-hiOLs at day 16 of trans-differentiation. Scale bars, 50 µm.

(C–H) Comparison of dc-hiOLs derived from one PMD patient with point mutation PLP1 643C>T with one control cell line. Percentage of $O4^+$ (C) and MBP^+ (D) cells at day 16. Data are shown as the mean + SEM of n = 3 different transdifferentiation experiments of one cell line for each group. Two-tailed unpaired t test was used for statistical analysis. (E) Representative plot profiles comparing the distribution of PLP1 in control (black) and PLP1 643C>T (green) dc-hiOLs. Two-dimensional graph of pixel intensity along cell diameter. (F) Apoptosis assay for PLP1 643C>T dc-hiOLs. MR-(DEVD)2 reagent is cleaved by active caspase-3/7 and produces a fluorescent product (magenta). ICC for $O4^+$

(legend continued on next page)

methylation dataset and confirmed the distinction of fibroblasts and the derived dc-hiOLs in separate age groups (Figure S5B). Overall, our results show that dc-hiOLs preserve the epigenetic age of donor cells, at least with respect to DNA methylation profile, and represent a promising model to study age-associated myelin deficits.

DISCUSSION

Limited access to human oligodendrocytes has been an obstacle in biomedical research of myelin disorders. Differentiation of human iPSCs into oligodendrocytes enables large-scale production of cells and provides a valuable tool in clinical research. However, this technology faces the challenges of high-cost, complex, and time-consuming cell-culture techniques and genetic instability (Popp et al., 2018). Our results suggest that direct conversion of fibroblasts into OLs is a rapid and inexpensive technique, which represents a complementary tool to study myelin diseases and identify remyelination-promoting compounds.

Ectopic expression of SON directly transdifferentiates human fibroblasts within 16 days into $O4^+$ dc-hiOLs, which exhibit oligodendroglial properties. Although the efficiency varies between fibroblast lines of different tissue origin, in the vast majority of the lines the efficiency is higher than in earlier protocols using mouse cells (Najm et al., 2013; Yang et al., 2013), which may be explained by the polycistronic construct used here and the thereby increased transduction efficiency as shown recently for directly converted neurons (Herdy et al., 2019). Notably, the fibroblast line that showed the lowest transdifferentiation efficiency was derived from lung tissue (Fib C, Figure 1C), in contrast to all other lines which originated from skin, suggesting that the source tissue might affect conversion efficiency; however, studies examining systematically the influence of tissue origin of fibroblasts on the transdifferentiation efficiency are currently lacking.

Gene expression and chromatin analysis revealed a chromatin switch that coincides with activation of the oligodendrocyte transcriptional program during reprogramming. Several members of the SOX TF family are among the top enriched TF motifs in induced oligodendrocytes. SOX10 is critical for the determination of oligodendroglial fate (Garcia-Leon et al., 2018), whereas SOX2 and SOX3 have been shown to play a redundant role in promoting oligodendrocyte differentiation partially through downregulation of miR-145 (Hoffmann et al., 2014). Furthermore, in spinal cord precursor cells SOX3 suppresses astrocytic genes, whereas SOX9 and SOX10 promote the differentiation into oligodendrocytes (Klum et al., 2018). We observed remaining activity of fibroblast TFs including the AP1 family, which may explain the incomplete silencing of the fibroblast program. However, we showed that the acquired oligodendroglial fate is stable and that cells do not revert back to fibroblast fate upon transgene silencing. Inhibition of AP1 activity and use of small molecules that regulate the epigenetic landscape of the donor cells might further increase the efficiency of oligodendroglial transdifferentiation, as has been recently shown for directly converted neurons (Herdy et al., 2019).

$O4^+$ dc-hiOLs can be easily purified and used for drug screens and testing of promyelinating compounds. We demonstrated that clemastine, benztropine, and miconazole increase significantly the terminal differentiation of dc-hiOLs into MBP^+ cells. Since fibroblasts differentiate rapidly into $O4^+$ dc-hiOLs, dc-hiOLs might be less suitable to identify compounds that have a positive effect on early oligodendroglial differentiation stages.

Reprogramming technology provides a unique opportunity to generate scarcely accessible cell types and study related disorders. As demonstrated here, dc-hiOLs can serve as a system for disease modeling of rare demyelinating diseases. PMD is a monogenic X-linked leukodystrophy related to PLP1 mutations. PLP1-related disorders are characterized by genetic heterogeneity reflected in a wide spectrum of pathology, ranging from absence of motor acquisition with early-age lethality (PMD form 0) to walking capacities with normal life expectancy (form 4 or SPG2) (Cailloux et al., 2000; Osorio and Goldman, 2018). We found that dc-hiOLs bearing the PLP1 643C>T mutation suffer from ER stress and exhibit impaired terminal differentiation to myelinogenic MBP^+ cells, whereas PLP1 duplication develops a milder phenotype. Our data confirm the results of prior publications studying iPSC-derived OLs from patients with PMD and provide evidence that dc-hiOLs are suitable for disease modeling and for the identification of correlations between genotypes and phenotypes (Madhavan et al., 2018; Nevin et al., 2017; Numasawa-Kuroiwa et al., 2014). The rapidity of the described protocol enables

(green) after apoptotic cell labeling at day 13. Scale bar, 75 μm. (G) Percentage of $O4^+$ dc-hiOLs with active caspase-3/7 at differentiation day 13. Cells were treated with DMSO vehicle (Control, PLP1 643C>T) or 1 μM GSK2656157 (PLP1 643C>T + GSK2656157) from differentiation day 5 onward to test for phenotype rescue. Data are shown as the mean + SEM of n = 3 transdifferentiation experiments. Two-tailed unpaired t test was used for statistical analysis. (H) Quantification of MBP^+ cells at day 16. PLP1 643C>T dc-hiOLs were treated with either vehicle (DMSO) or 1 μM GSK2656157 from differentiation day 5 onward. Data are presented as the mean + SEM of n = 3 different transdifferentiation experiments. Unpaired Student's t test was used for statistical analysis.
*$p < 0.05$, **$p < 0.01$. See also Figure S4.

Please cite this article in press as: Chanoumidou et al., One-step Reprogramming of Human Fibroblasts into Oligodendrocyte-like Cells by SOX10, OLIG2, and NKX6.2, Stem Cell Reports (2021), https://doi.org/10.1016/j.stemcr.2021.03.001

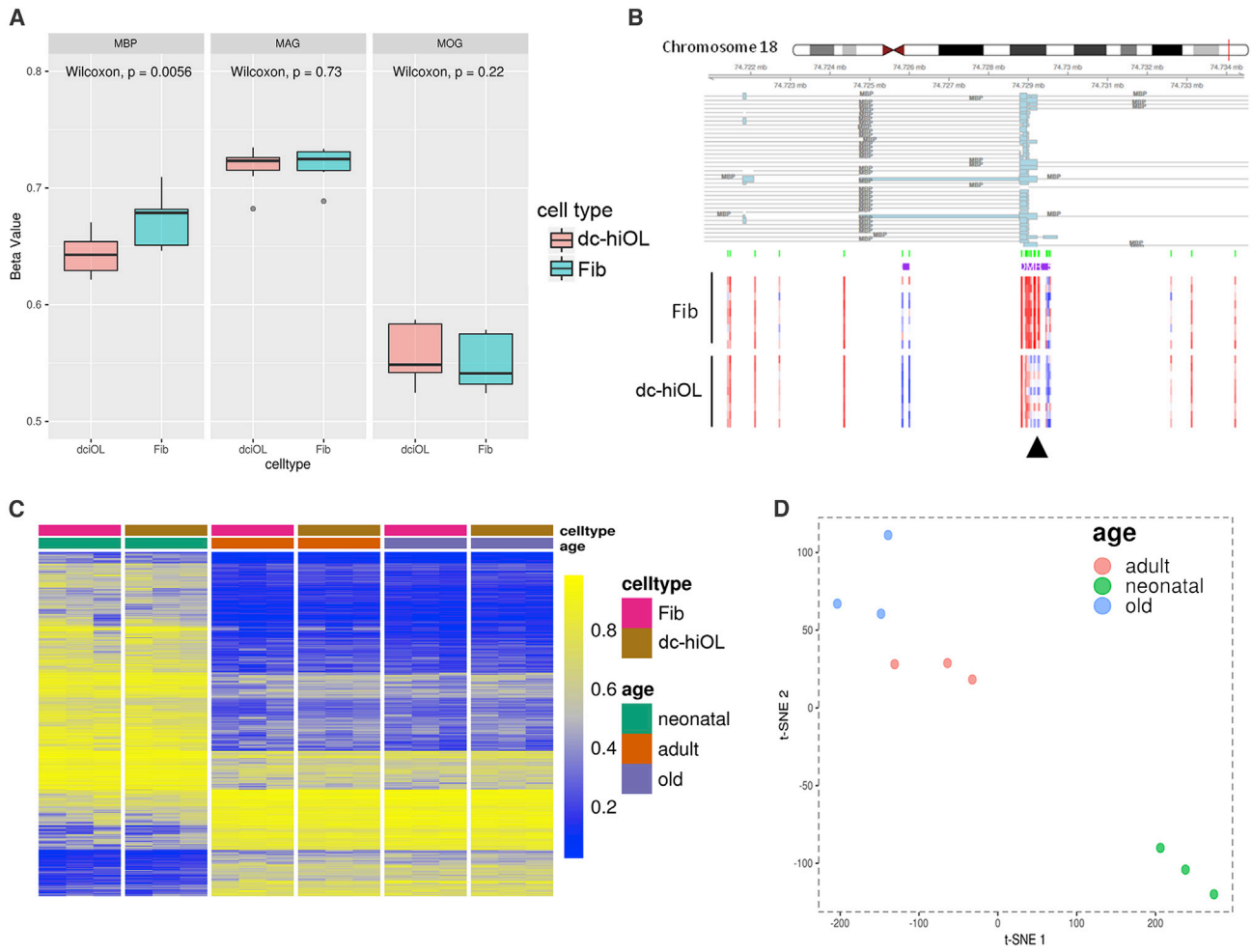

Figure 5. Epigenetic Characterization of Fibroblast and dc-hiOL Samples

(A) Focused analysis of methylation β values of CpG sites mapping to *MBP*, *MAG*, and *MOG* genes showing that only *MBP* is differentially methylated on the global gene level between dciOL and fibroblast samples ($p < 0.01$, Wilcoxon's test).

(B) Unsupervised analysis of differentially methylated regions between dciOL and fibroblast samples revealed a region of 17 CpG sites mapping to exon 1 (hg19 coordinates: chr18:74,728,834-74,729,551) of *MBP* transcripts typically expressed in the brain being hypomethylated in dc-hiOL samples as compared with fibroblast samples (HMM-Fisher, $p = 1 \times 10^{-19}$).

(C) Heatmap showing methylation β values of the top 1,000 differentially methylated probes between aged samples and neonatal samples. Note the shared aging signature between fibroblast and dc-hiOL samples across neonatal and aged samples.

(D) Unsupervised t-distributed stochastic neighbor embedding (t-SNE) analysis of all dc-hiOL samples showing that aged and old samples group together and are clearly separated from neonatal samples.

See also Figure S5.

generation of dc-hiOLs from numerous patients at low cost, providing a platform for studying additional myelin or CNS diseases and the identification of clinical subgroups. dc-hiOLs might have the potential to facilitate the development of personalized medicine by bypassing the relative expensive and time-consuming generation of iPSCs. A key feature of dc-hiOLs, as revealed by CpG methylation analysis, is that cells circumvent rejuvenation and retain the epigenetic age of donor cells. Aging is a major risk for many CNS diseases, and our data suggest the applicability of dc-hiOLs in studies of age-related myelin alterations. However, assessment of additional age-related features such as mitochondrial and telomerase activity needs to be performed for future use of dc-hiOLs in aging studies. A limitation of the available transdifferentiation methods, including ours, is the limited yield of produced cells due to the lack of an intermediate stem cell type, restricting the conduction of large-scale assays. An alternative strategy for the generation of human OLs is represented by the reprogramming of

fibroblasts into induced neural progenitor cells (iNPCs) and subsequent differentiation into oligodendrocytes (Meyer et al., 2014). Additional studies comparing side-by-side oligodendrocytes generated from fibroblasts, iNPCs, or iPSCs will help to further evaluate the advantages and disadvantages of the different techniques. Of note, although the *in vitro* data provided here support the oligodendroglial identity of dc-hiOLs, further analysis of their capacity to form compact myelin sheaths *in vivo* is needed.

In summary, direct conversion of fibroblasts into dc-hiOLs represents a rapid, efficient, and inexpensive alternative to iPSC-derived human oligodendrocytes for disease modeling and the identification of remyelination-promoting compounds, and advances significantly the possibility of personalized medicine in the field of de- and dysmyelinating diseases.

EXPERIMENTAL PROCEDURES

Plasmids and Lentiviral Preparation

The construction of the polycistronic lentiviral SF-SON-puro and SF-SON-RFP vectors has been previously described (Ehrlich et al., 2017). Detailed description of the plasmids and the lentiviral production can be found in supplemental experimental procedures.

Cell Lines and Culture

A summary of the cell lines used in this study is provided in Table S2. Detailed description can be found in supplemental experimental procedures.

Direct Conversion of Fibroblasts to dc-hiOLs

Fibroblasts were seeded at a density of 12×10^3 cells/cm^2 on a poly-L-lysine (Sigma)/mouse laminin (Sigma) coated plate in fibroblast medium (FM). The next day cells were transduced with the SF-SON lentivirus in fresh FM, and 16 h later the medium was changed to glial induction medium (GIM), which consisted of DMEM-F12 (Gibco), 1:200 N2 supplement (Gibco), 1:100 B27 supplement lacking vitamin A (Gibco), and 1% penicillin/streptomycin/glutamine (Sigma) supplemented with 0.5 μM Smoothened agonist (SAG) (Cayman Chemical), 10 ng/mL platelet-derived growth factor (PDGF) (Peprotech), 200 μM ascorbic acid (AA) (Sigma), and 20 ng/mL T3 (Sigma). GIM was changed every other day and the concentration of T3 was increased to 60 ng/mL at day 4. Puromycin (1 μg/mL, Gibco) selection of the transduced cells took place for the first 5 days. At day 9 the GIM was replaced by glial differentiation medium (GDM) consisting of DMEM-F12, 1:200 N2 supplement, 1:100 B27 supplement lacking vitamin A, 1% penicillin/streptomycin/glutamine enriched by 0.5 μM SAG, 60 ng/mL T3, 10 ng/mL NT3 (Peprotech), 10 ng/mL IGF-1 (Peprotech), 200 μM AA, and 10 ng/mL PDGF. PDGF was replaced by 100 μM dbcAMP (Sigma) at day 12. Medium change was performed every other day. Cells of low passage (fewer than 10) were used for all direct reprogramming experiments. Conversion efficiency is defined as the number of O4$^+$ cells divided by the total number of 4′,6-diamidino-2-phenylindole (DAPI)-positive cells at day 16. Yield is defined as the number of O4$^+$ cells at day 16 divided by the number of plated fibroblasts at day 0.

Immunocytochemistry

Cells were fixed using 4% paraformaldehyde (PFA) for 20 min and permeabilized with 0.5% Triton X-100 solution for 10 min. For O4 no cell permeabilization was performed. After three PBS washes, cells were blocked for 30 min with 5% normal goat serum and 5% fetal bovine serum in PBS. Primary antibodies were added in blocking buffer overnight at 4°C. Upon three washes, the secondary antibodies were added in PBS at room temperature for 2 h. Nuclei were stained with1 μg/mL DAPI (Sigma-Aldrich). Cells on glass coverslips were visualized on a Zeiss LSM700 confocal microscope, while cells cultured on a plastic surface were visualized on a Leica DMI6000 B inverted microscope. The primary antibodies are listed in Table S3. Anti-PLP1 antibody was generously provided by Prof. Bruce Trapp.

Flow Cytometry

Details of flow cytometry are provided in supplemental experimental procedures.

Migration Assay

The methodology of migration assay is described in supplemental experimental procedures.

Isolation of Primary Human Oligodendrocytes

Brain tissue was obtained from adults undergoing surgical resections as treatment for non-tumor-related intractable epilepsy in accordance with the guidelines set by the Biomedical Ethics Unit of McGill University. Details are provided in supplemental experimental procedures.

Quantitative RT-PCR

Total RNA was extracted from cells using the RNeasy Mini Kit (Qiagen). DNase (Qiagen) treatment was used to avoid genomic DNA contamination, and RNA was reversely transcribed to cDNA using the High Capacity cDNA Reverse Transcription Kit (Applied Biosystems). qRT-PCR was carried out using SYBR Green-based detection and gene expression was normalized to GAPDH. The primers can be found in Table S3.

RNA-seq, ATAC-seq, and DNA Methylation Array Analysis

The methodology of RNA-seq, ATAC-seq, and DNA methylation analysis is described in supplemental experimental procedures.

In Vitro Myelination Assays

Nanofiber chamber slides (PCL NanoAligned) were coated with FITC-conjugated poly-L-lysine (Sigma) for 2 h at 37°C followed by two washes with sterile H_2O and overnight incubation with mouse laminin (Sigma) at 4°C. Twenty-four hours before cell plating, nanofibers were incubated with GDM at 37°C. O4-expressing dc-hiOLs were purified at day 11 of the transdifferentiation process and replated on the nanofiber slides (60,000 cells/slide)

in GDM. Half-medium change was performed every other day and cells were analyzed with ICC after 10 days. A published heuristic algorithm was used to analyze the morphology of dc-hiOLs and iPSC-derived hiOLs on nanofibers (Xu et al., 2019). Three-dimensional reconstruction of confocal image stacks was performed with IMARIS analysis software (Oxford Instruments). 3D surface rendering was applied.

For the neuronal/dc-hiOL co-culture experiments, neurons were generated from human iPSC-derived NPC as previously described (Ehrlich et al., 2017) and replated at densities of 2×10^5 per well in 24-well plates containing Matrigel-coated (BD Biosciences) glass coverslips. After 22 days of differentiation, neurons were used for co-culture assays. dc-hiOLs purified for O4 at day 11 of transdifferentiation were added to 22-day-old neurons at densities of 9×10^4 cells per well in 24-well plates. Co-cultures were maintained in GDM supplemented with 2 ng/mL brain-derived neurotrophic factor (Peprotech) and 2 ng/mL glial cell line-derived neurotrophic factor (Peprotech). Following 6 days of co-culture, cells were fixed in 4% PFA for ICC analysis.

Compound Treatment

Methodological details are provided in supplemental experimental procedures.

Apoptosis Assay

A Magic Red Caspase3/7 Assay Kit (Bio-Rad) was used for measurement of caspase activity. Further details are provided in supplemental experimental procedures.

Statistics

Data of at least three biological replicates (n) are presented as the mean ± SEM. Statistical significance was determined by Student's t test. Significance was set at $*p < 0.05$, $**p < 0.01$, and $***p < 0.001$.

Data and Code availability

The accession number for the RNA-seq data reported in this paper is ArrayExpress: E-MTAB-7838. The RNA-seq data and will be made publicly available upon publication. The R script for the comparison of our RNA-seq data with the published dataset by Jäkel et al. (2019) is available on github (https://github.com/ctho1/compareRNAseq).

SUPPLEMENTAL INFORMATION

Supplemental Information can be found online at https://doi.org/10.1016/j.stemcr.2021.03.001.

AUTHOR CONTRIBUTIONS

T.K., K.C., and M.E. conceived the study; B.H.-R. and J.M.V. designed and analyzed the RNA-seq and ATAC-seq experiments; C.T. performed biostatistical analyses; K.C., F.W., S.A., M.S., S.V., Q.L.C., and M.E. performed the *in vitro* experiments; K.C., S.M., A.B.-V.E., and Y.K.T.X. analyzed data; O.B.-T. provided the PMD duplicated fibroblasts and clinical expertise; J.A., G.M., L.O., J.W., and K.-P.K. provided human cells/cell lines; K.C. and T.K. drafted the manuscript; B.H.-R., L.O., H.R.S., A.B.-V.E., O.B.-T., J.M.V., and M.E. were involved in editing and discussion.

CONFLICTS OF INTEREST

T.K. and M.E. have filed a patent for the generation of human oligodendrocytes. T.K. received compensation for serving on scientific advisory boards (Frequency Therapeutics, Inc.) and speaker honoraria and research funding from Novartis.

ACKNOWLEDGMENTS

We thank Dr. Thomas Zobel from the Imaging Network, Münster for helping with the 3D reconstruction analysis and Dr. Laura Starost for providing hiOLs. This work was supported by the German Research Foundation (DFG CRC-TR-128B07 to T.K.), Interdisciplinary Center for Clinical Research (KuT3/007/20 to T.K.), Progressive MS Alliance (collaborative research network PA-1604-08492 (BRAVEinMS) to G.M., J.A., A.B.-V.E., and T.K.), AFM-TELETHON 20270 (to A.B.-V.E.), the National MS Society (RG-1801-30020 to T.K.), and the EC FP7 project LEUKOTREAT and "les amis de Ianis" association (to O.B.-T.). Work in the Vaquerizas laboratory was funded by the Max Planck Society, the Deutsche Forschungsgemeinschaft (DFG) Priority Program SPP 2202 'Spatial Genome Architecture in Development and Disease' (project no. 422857230 to J.M.V.), the DFG Clinical Research Unit CRU326 'Male Germ Cells: from Genes to Function' (project no. 329621271 to J.M.V.), the European Union's Horizon 2020 research and innovation program under the Marie Skłodowska-Curie grant agreement no. 643062—ZENCODE-ITN to J.M.V., and the Medical Research Council, UK.

Received: March 22, 2020
Revised: March 1, 2021
Accepted: March 1, 2021
Published: March 25, 2021

REFERENCES

Cailloux, F., Gauthier-Barichard, F., Mimault, C., Isabelle, V., Courtois, V., Giraud, G., Dastugue, B., and Boespflug-Tanguy, O. (2000). Genotype-phenotype correlation in inherited brain myelination defects due to proteolipid protein gene mutations. Clinical European Network on Brain Dysmyelinating Disease. Eur. J. Hum. Genet. *8*, 837–845.

Deshmukh, V.A., Tardif, V., Lyssiotis, C.A., Green, C.C., Kerman, B., Kim, H.J., Padmanabhan, K., Swoboda, J.G., Ahmad, I., Kondo, T., et al. (2013). A regenerative approach to the treatment of multiple sclerosis. Nature *502*, 327–332.

Douvaras, P., and Fossati, V. (2015). Generation and isolation of oligodendrocyte progenitor cells from human pluripotent stem cells. Nat. Protoc. *10*, 1143–1154.

Ehrlich, M., Mozafari, S., Glatza, M., Starost, L., Velychko, S., Hallmann, A.L., Cui, Q.L., Schambach, A., Kim, K.P., Bachelin, C., et al. (2017). Rapid and efficient generation of oligodendrocytes from human induced pluripotent stem cells using transcription factors. Proc. Natl. Acad. Sci. U S A *114*, E2243–E2252.

Fraga, M.F., and Esteller, M. (2007). Epigenetics and aging: the targets and the marks. Trends Genet. *23*, 413–418.

Franklin, R.J.M., and Ffrench-Constant, C. (2017). Regenerating CNS myelin—from mechanisms to experimental medicines. Nat. Rev. Neurosci. *18*, 753–769.

Garcia-Leon, J.A., Kumar, M., Boon, R., Chau, D., One, J., Wolfs, E., Eggermont, K., Berckmans, P., Gunhanlar, N., De Vrij, F., et al. (2018). SOX10 single transcription factor-based fast and efficient generation of oligodendrocytes from human pluripotent stem cells. Stem Cell Rep. *10*, 655–672.

Heinz, S., Benner, C., Spann, N., Bertolino, E., Lin, Y.C., Laslo, P., Cheng, J.X., Murre, C., Singh, H., and Glass, C.K. (2010). Simple combinations of lineage-determining transcription factors prime cis-regulatory elements required for macrophage and B cell identities. Mol. Cell *38*, 576–589.

Herdy, J., Schafer, S., Kim, Y., Ansari, Z., Zangwill, D., Ku, M., Paquola, A., Lee, H., Mertens, J., and Gage, F.H. (2019). Chemical modulation of transcriptionally enriched signaling pathways to optimize the conversion of fibroblasts into neurons. eLife *8*, e41356.

Hoffmann, S.A., Hos, D., Kuspert, M., Lang, R.A., Lovell-Badge, R., Wegner, M., and Reiprich, S. (2014). Stem cell factor Sox2 and its close relative Sox3 have differentiation functions in oligodendrocytes. Development *141*, 39–50.

Horvath, S. (2013). DNA methylation age of human tissues and cell types. Genome Biol. *14*, R115.

Huh, C.J., Zhang, B., Victor, M.B., Dahiya, S., Batista, L.F., Horvath, S., and Yoo, A.S. (2016). Maintenance of age in human neurons generated by microRNA-based neuronal conversion of fibroblasts. eLife *5*, e18648.

Jäkel, S., Agirre, E., Mendanha Falcao, A., Van Bruggen, D., Lee, K.W., Knuesel, I., Malhotra, D., Ffrench-Constant, C., Williams, A., and Castelo-Branco, G. (2019). Altered human oligodendrocyte heterogeneity in multiple sclerosis. Nature *566*, 543–547.

Klum, S., Zaouter, C., Alekseenko, Z., Bjorklund, A.K., Hagey, D.W., Ericson, J., Muhr, J., and Bergsland, M. (2018). Sequentially acting SOX proteins orchestrate astrocyte- and oligodendrocyte-specific gene expression. EMBO Rep. *19*, e46635.

Lapasset, L., Milhavet, O., Prieur, A., Besnard, E., Babled, A., It-Hamou, N., Leschik, J., Pellestor, F., Ramirez, J.M., De, V.J., et al. (2011). Rejuvenating senescent and centenarian human cells by reprogramming through the pluripotent state. Genes Dev. *25*, 2248–2253.

Madhavan, M., Nevin, Z.S., Shick, H.E., Garrison, E., Clarkson-Paredes, C., Karl, M., Clayton, B.L.L., Factor, D.C., Allan, K.C., Barbar, L., et al. (2018). Induction of myelinating oligodendrocytes in human cortical spheroids. Nat. Methods *15*, 700–706.

Matjusaitis, M., Wagstaff, L.J., Martella, A., Baranowski, B., Blin, C., Gogolok, S., Williams, A., and Pollard, S.M. (2019). Reprogramming of fibroblasts to oligodendrocyte progenitor-like cells using CRISPR/Cas9-Based synthetic transcription factors. Stem Cell Rep. *13*, 1053–1067.

Meissner, A., Mikkelsen, T.S., Gu, H., Wernig, M., Hanna, J., Sivachenko, A., Zhang, X., Bernstein, B.E., Nusbaum, C., Jaffe, D.B., et al. (2008). Genome-scale DNA methylation maps of pluripotent and differentiated cells. Nature *454*, 766–770.

Mertens, J., Paquola, A.C., Ku, M., Hatch, E., Bohnke, L., Ladjevardi, S., Mcgrath, S., Campbell, B., Lee, H., Herdy, J.R., et al. (2015). Directly reprogrammed human neurons retain aging-associated transcriptomic signatures and reveal age-related nucleocytoplasmic defects. Cell Stem Cell *17*, 705–718.

Meyer, K., Ferraiuolo, L., Miranda, C.J., Likhite, S., Mcelroy, S., Renusch, S., Ditsworth, D., Lagier-Tourenne, C., Smith, R.A., Ravits, J., et al. (2014). Direct conversion of patient fibroblasts demonstrates non-cell autonomous toxicity of astrocytes to motor neurons in familial and sporadic ALS. Proc. Natl. Acad. Sci. U S A *111*, 829–832.

Micu, I., Plemel, J.R., Caprariello, A.V., Nave, K.A., and Stys, P.K. (2018). Axo-myelinic neurotransmission: a novel mode of cell signalling in the central nervous system. Nat. Rev. Neurosci. *19*, 49–58.

Najm, F.J., Lager, A.M., Zaremba, A., Wyatt, K., Caprariello, A.V., Factor, D.C., Karl, R.T., Maeda, T., Miller, R.H., and Tesar, P.J. (2013). Transcription factor-mediated reprogramming of fibroblasts to expandable, myelinogenic oligodendrocyte progenitor cells. Nat. Biotechnol. *31*, 426–433.

Najm, F.J., Madhavan, M., Zaremba, A., Shick, E., Karl, R.T., Factor, D.C., Miller, T.E., Nevin, Z.S., Kantor, C., Sargent, A., et al. (2015). Drug-based modulation of endogenous stem cells promotes functional remyelination in vivo. Nature *522*, 216–220.

Nevin, Z.S., Factor, D.C., Karl, R.T., Douvaras, P., Laukka, J., Windrem, M.S., Goldman, S.A., Fossati, V., Hobson, G.M., and Tesar, P.J. (2017). Modeling the mutational and phenotypic landscapes of Pelizaeus-Merzbacher disease with human iPSC-derived oligodendrocytes. Am. J. Hum. Genet. *100*, 617–634.

Numasawa-Kuroiwa, Y., Okada, Y., Shibata, S., Kishi, N., Akamatsu, W., Shoji, M., Nakanishi, A., Oyama, M., Osaka, H., Inoue, K., et al. (2014). Involvement of ER stress in dysmyelination of Pelizaeus-Merzbacher disease with PLP1 missense mutations shown by iPSC-derived oligodendrocytes. Stem Cell Rep. *2*, 648–661.

Osorio, M.J., and Goldman, S.A. (2018). Neurogenetics of Pelizaeus-Merzbacher disease. Handb Clin. Neurol. *148*, 701–722.

Popp, B., Krumbiegel, M., Grosch, J., Sommer, A., Uebe, S., Kohl, Z., Plotz, S., Farrell, M., Trautmann, U., Kraus, C., et al. (2018). Need for high-resolution genetic analysis in iPSC: results and lessons from the ForIPS consortium. Sci. Rep. *8*, 17201.

Pouya, A., Rassouli, H., Rezaei-Larijani, M., Salekdeh, G.H., and Baharvand, H. (2020). SOX2 protein transduction directly converts human fibroblasts into oligodendrocyte-like cells. Biochem. Biophys. Res. Commun. *525*, 1–7.

Stangel, M., Kuhlmann, T., Matthews, P.M., and Kilpatrick, T.J. (2017). Achievements and obstacles of remyelinating therapies in multiple sclerosis. Nat. Rev. Neurol. *13*, 742–754.

Van Der Knaap, M.S., and Bugiani, M. (2017). Leukodystrophies: a proposed classification system based on pathological changes and pathogenetic mechanisms. Acta Neuropathol. *134*, 351–382.

Xu, Y.K.T., Chitsaz, D., Brown, R.A., Cui, Q.L., Dabarno, M.A., Antel, J.P., and Kennedy, T.E. (2019). Deep learning for high-throughput quantification of oligodendrocyte ensheathment at single-cell resolution. Commun. Biol. *2*, 116.

Yang, N., Zuchero, J.B., Ahlenius, H., Marro, S., Ng, Y.H., Vierbuchen, T., Hawkins, J.S., Geissler, R., Barres, B.A., and Wernig, M. (2013). Generation of oligodendroglial cells by direct lineage conversion. Nat. Biotechnol. *31*, 434–439.

Stem Cell Reports, Volume *16*

Supplemental Information

One-step Reprogramming of Human Fibroblasts into Oligodendrocyte-like Cells by SOX10, OLIG2, and NKX6.2

Konstantina Chanoumidou, Benjamín Hernández-Rodríguez, Farina Windener, Christian Thomas, Martin Stehling, Sabah Mozafari, Stefanie Albrecht, Linda Ottoboni, Jack Antel, Kee-Pyo Kim, Sergiy Velychko, Qiao Ling Cui, Yu Kang T. Xu, Gianvito Martino, Jürgen Winkler, Hans R. Schöler, Anne Baron-Van Evercooren, Odile Boespflug-Tanguy, Juan M. Vaquerizas, Marc Ehrlich, and Tanja Kuhlmann

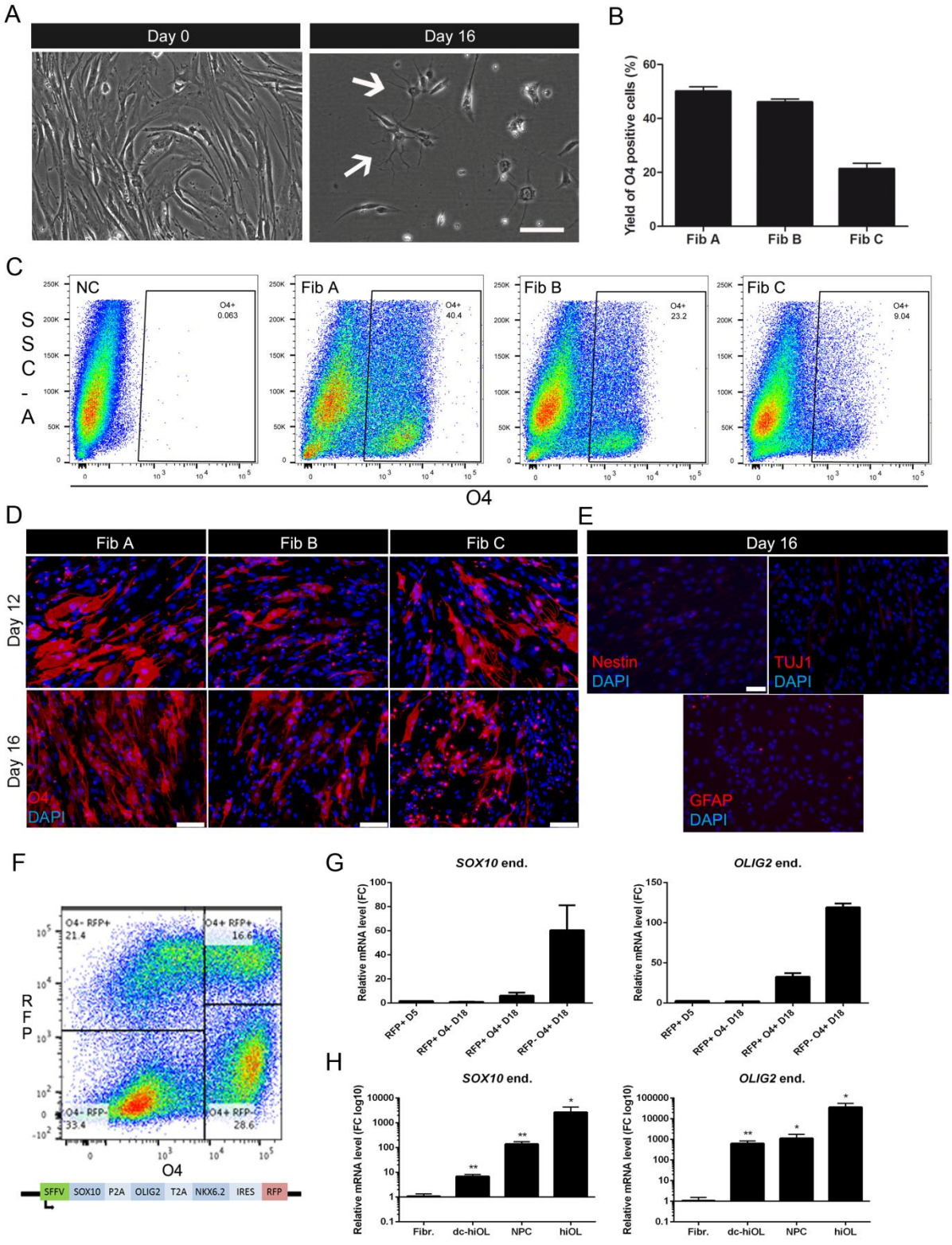

Figure S1: Analysis of the direct conversion process. Related to Figure 1.

A) Bright field photos showing fibroblasts at day 0 and purified O4+ cells at day 16 of differentiation. White arrows indicate cells with oligodendrocyte-like morphology. Scale Bar: 50µm. **B)** Yield of O4+ dc-hiOLs derived from Fib A, B and C at day 16 defined as the number of O4+ cells divided by the number of plated fibroblasts. Data are presented as the mean +SEM of n=3 different transdifferentiation experiments for each cell line. **C)** Representative flow cytometry analyses for O4 at day 16 postinfection of Fib A, B and C with SON or control (NC) lentivirus. **D)** Immunofluorescence images of O4+ cells (red) derived from Fib A, B and C at days 12 and 16 post-infection. Scale Bar: 100µm. **E)** Immunostaining of dc-hiOLs for Nestin, TUJ1 and GFAP (red) at day 16

post-infection. Scale Bar: 75µm. **F)** Fibroblasts were infected with SON-IRES-RFP lentivirus enabling detection of transgene expression. Flow cytometry analysis for O4 and RFP in neonatal fibroblasts infected with SON-RFP lentivirus at day 16 identifies RFP- and O4+ cells in addition to RFP- O4-; RFP+ O4- and RFP+ O4+. **G)** Quantitative RT-PCR analysis showing the upregulation of endogenous Sox10 and Olig2 transcripts in dc-hiOLs at reprogramming day 18 in both virus-silenced (RFP-O4+) and non-silenced (RFP+O4+) cells. Gene expression at day 18 was normalized to day 5. FC: fold change. Data are shown as mean +SEM of n=3 technical replicated of one cell line. **H)** Quantitative RT-PCR for endogenous *SOX10* and *OLIG2* in human fibroblasts (Fibr.), dc-hiOLs, neural progenitor cells (NPC) and iPSC-derived oligodendrocytes (hiOL). Data are presented as fold change (FC) difference to fibroblasts. mean+SEM of 3 three different cell lines. Unpaired t-test was used for statistical analysis.

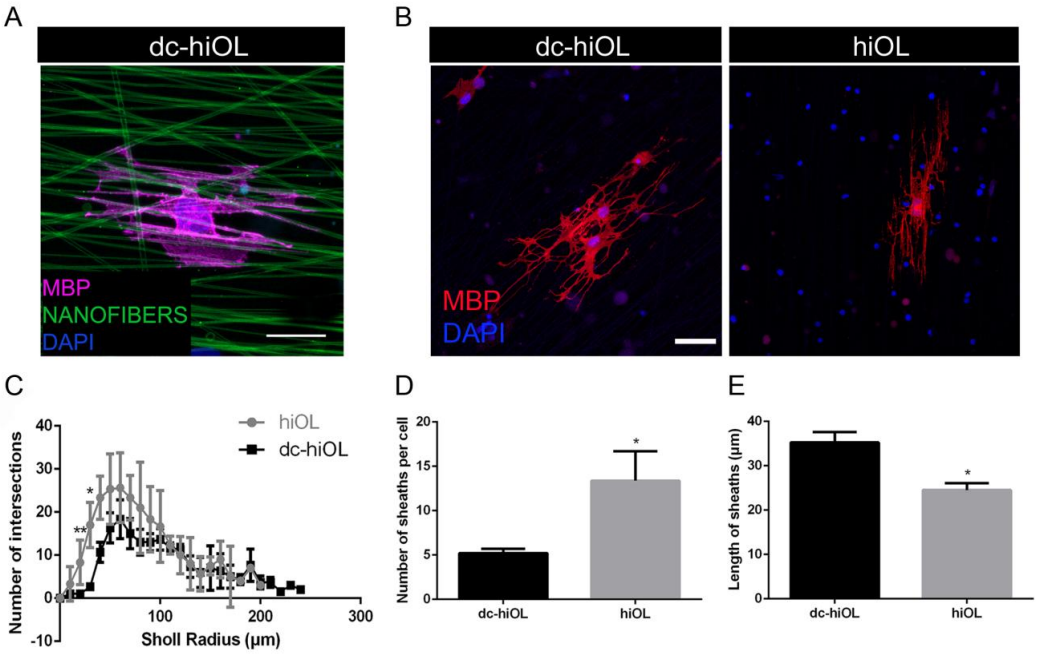

Figure S2: Morphological comparison of dc-hiOLs with iPSC-derived hiOLs. Related to Figure 1.

Purified O4+ cells were cultured on nanofibers for 10 days. Cell morphology was assesed with immunostaining for MBP. **A)** Confocal picture of dc-hiOLs stained for MBP (magenta) and cultured on FITC labeled nanofibers (green). This photo was used for 3D recostruction shown in Figure 1.Scale bar:10µm. **B)** Immunostaining of dc-hiOLs and hiOLs cultured on nanofibers for MBP. Scale Bar:100µm. **C)** Sholl analysis of dc-hiOLs and hiOLs. Sholl intersection profile is obtained by counting the numbers of cellular intersections that defined distances from the soma in concentric circles. Analysis was performed with Image J. n=3 different cell lines for each group. 10 cells were counted for each cell line. **D,E)** Comparison of the number (D) and length (E) of sheaths formed by dc-hiOLs and hiOLs cultured on nanofibers as analyzed with a heuristic algorithm (Xu et al., 2019). n=3 different cell lines for each group. 11 cells were counted for each cell line.

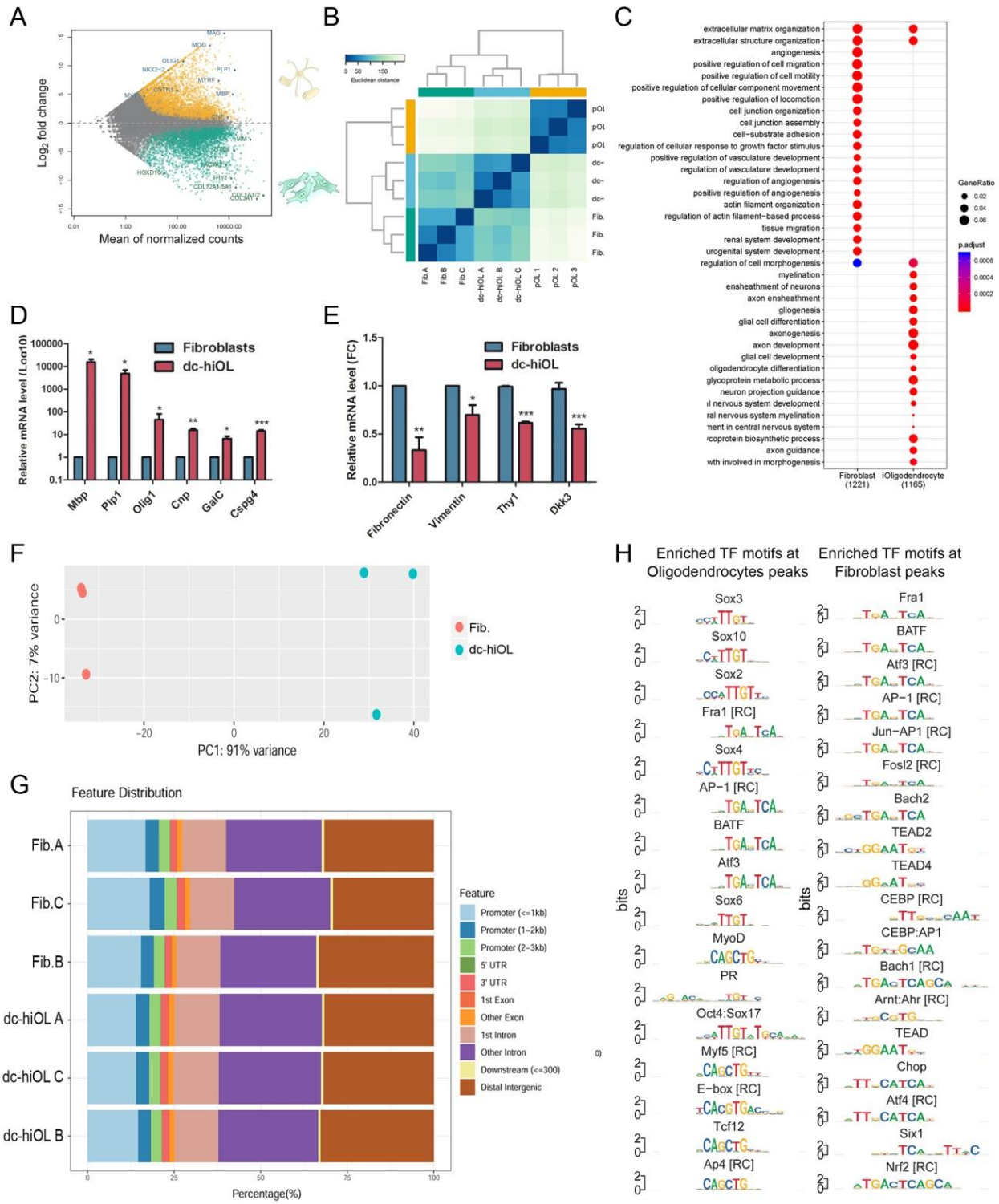

Figure S3: Transcriptomic profiling and changes in chromatin accessibility during reprogramming to dc-hiOLs. Related to Figure 2.

A) MA plot comparing primary oligodendrocytes and fibroblasts. Differentially expressed genes with an FDR < 0.01 are color-coded. Yellow dots, primary oligodendrocyte up-regulated genes (5899); light green dots, fibroblast-upregulated genes (5257); dark blue dots, representative oligodendrocyte marker genes; dark green dots, representative fibroblast marker genes. **B)** Unsupervised hierarchical clustering of normalized counts from the top 1000 most variable genes. The color scale reflects Euclidean distance among the samples. Fib: fibroblasts; dc-hiOLs: directly converted induced oligodendrocytes; pOL: primary oligodendrocytes **C)** Dot plot showing top enriched gene ontology terms with FDR < 0.01. Dot size is proportional to the percentage of annotated genes inside the term that are also inside the up-regulated or down-regulated groups. Color is

proportional to multiple-testing-corrected significance values. **D,E)** Quantitative RT-PCR analysis of representative oligodendrocyte (D) and fibroblast (E) genes in fibroblasts and dc-hiOLs at day 16. Data are shown as the average + SEM of n=3 different cell lines. One-tailed (D) and two-tailed (E) unpaired t-tests were used for statistical analysis. **F)** Principal component analysis of ATAC-seq samples showing the high reproducibility between biological replicates. **G)** Genomic distribution of ATAC-seq peaks with respect to annotated genes showing a high occurrence at promoter and intronic regions. **H)** Left, Top enriched motifs at dc-hiOL accessible peaks shown in Figure 3. Enrichment was assessed by HOMER (Heinz et al., 2010) and motifs with FDR< 0.05 are shown. Right, Top enriched motifs (FDR< 0.05) at fibroblast accessible peaks.

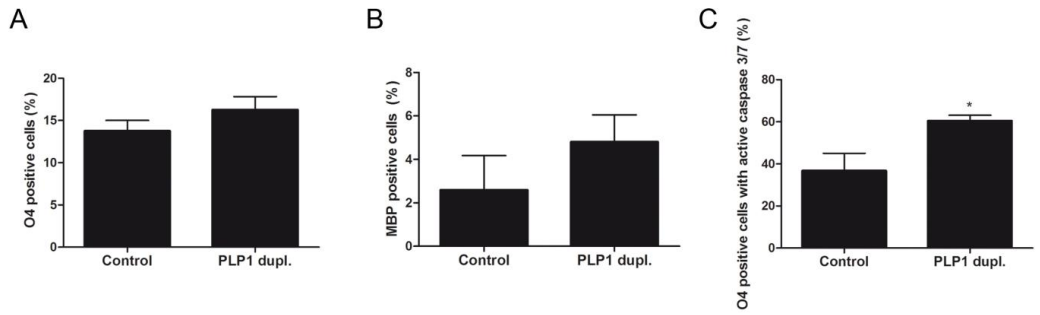

Figure S4: *PLP1* duplication does not affect significantly the differentiation of dc-hiOLs into MBP+ oligodendrocytes. Related to Figure 4.

Three PLP1 dupl. cell lines were compared with two sex and age matched controls. **A,B)** Percentage of O4+ (A) and MBP+ (B) dc-hiOLs based on immunocytochemistry analysis at day 16. Data are shown as the average +SEM of n=3 different transdifferentiation experiments for each tested cell line. Two-tailed unpaired t-test was used for statistical analysis. **C)** Apoptosis assay based on the activity of Caspase3/7. Percentage of apoptotic O4+ cells at day 13 of transdifferentiation. Data are shown as the average +SEM of n=3 transdifferentiation experiments. Two-tailed unpaired t-test was used for statistical analysis.

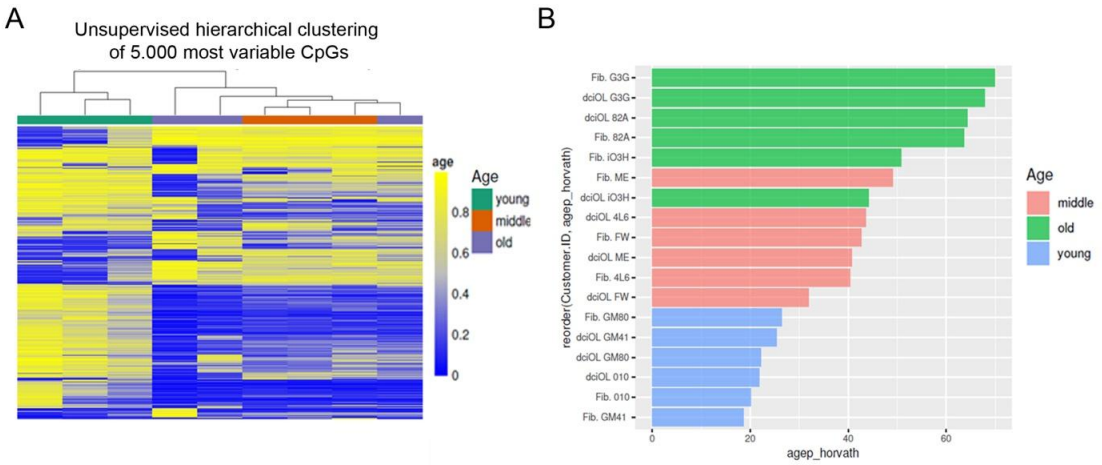

Figure S5: DNA methylation analysis shows age-associated changes in dc-hiOL samples. Related to Figure 5.

A) Unsupervised hierarchical clustering of the top 5.000 most variable CpGs across all dc-hiOL samples clearly separated neonatal samples from adult and old aged donors. **B)** Age prediction using Horvath's epigenetic clock confirmed the distinction of fibroblasts and the derived dc-hiOLs in separate age groups.

Table S1: Gene ontology analysis of significantly hypermethylated CpG sites comparing adult/old with neonatal samples (FDR<0.05). Provided separately as Excel file. Related to Figure 5.

Table S2: Summary of cell lines.

Cell line	Tissue of origin	Health condition	Age	Sex	Assay
PCS-201-010 (Fib A)	Skin	Healthy	Neonatal	Male	Transdifferentiation efficiency, DNA methylation assay, Compound test, Migration assay, Myelination assay, Test of transgene silencing, RNA-Seq, ATAC-Seq, Apoptosis assay (Control for PMDm1,2,3)
CRL-2097 (Fib B)	Skin	Healthy	Neonatal	Male	Transdifferentiation efficiency, RNA-Seq, ATAC-Seq, Apoptosis assay (Control for PMDm1,2,3)
CCL-153 (Fib C)	Lung	Healthy	Fetal	Male	Transdifferentiation efficiency, RNA-Seq, ATAC-Seq
UKM-F5BD	Skin	Healthy	47Y	Female	Transdifferentiation efficiency
UKERi-7MN	Skin	Healthy	52Y	Female	Transdifferentiation efficiency
UKERf-O3H	Skin	Healthy	71Y	Male	Transdifferentiation efficiency, DNA methylation assay
UKERf-82A	Skin	Healthy	66Y	Female	Transdifferentiation efficiency, DNA methylation assay
GM09546	Skin	Pelizaeus-Merzbacher Disease 643C>T	20Y	Male	Transdifferentiation efficiency, Apoptosis assay
PMDm1	Skin	Pelizaeus-Merzbacher Disease (PLP1dupl.)	3Y	Male	Transdifferentiation efficiency, Apoptosis assay
PMDm2	Skin	Pelizaeus-Merzbacher Disease (PLP1 dupl.)	3Y	Male	Transdifferentiation efficiency, Apoptosis assay
PMDm3	Skin	Pelizaeus-Merzbacher Disease (PLP1dupl.)	3Y	Male	Transdifferentiation efficiency, Apoptosis assay
GM00041	Skin	Healthy	3M	Female	DNA methylation assay, Myelination assay
GM08680	Skin	Healthy	5M	Male	DNA methylation assay. Myelination assay
GM22222	Skin	Healthy	1 DA	Male	Nanofibers, Compound test
GM08429	Skin	Healthy	1 DA	Male	Compound test
GM08447	Skin	Healthy	2 DA	Female	Compound test
UKERf-4L6	Skin	Healthy	32Y	Male	DNA methylation assay
UKM-F4AC	Skin	Healthy	32Y	Male	Transdifferentiation efficiency, DNA methylation assay, Transdifferentiation efficiency, Apoptosis assay (Control of GM09546)
UKM-F1AB	Skin	Healthy	25Y	Female	DNA methylation assay
UKER-fG3G	Skin	Healthy	69Y	Female	DNA methylation assay

Y=year, M= month, DA= day

Table S3: Primary antibodies for ICC and primer sequences for quantitative RT-PCR. Related to Figures: 1, 3, 4,S1,S2, S3.

Primary antibodies for Immunocytochemistry.			
Antibody	**Dilution**	**Company/Source**	**RRID**
Mouse anti-NESTIN	1:300	R&D (MAB1259)	AB_2251304
Mouse anti-O4	1:100	R&D (MAB1326)	AB_357617
Mouse anti-GALC	1:100	Millipore (MAB342)	AB_94857
Rat anti-MBP	1:50	Abcam (AB7349)	AB_305869
Rabbit anti–Ki-67	1:250	Abcam (AB16667)	AB_302459
Mouse anti-CNP	1:250	BioLegend (836401)	AB_2565361
Rabbit anti-PLP1	1:100	Provided by Prof. Bruce Trapp	
Mouse anti-TUBBIII (TUJ1)	1:750	Covance (MMS-435P)	AB_2313773
Mouse anti-GFAP	1:4.000	DAKO (Z0334)	AB_10013382

Primer sequences for quantitative RT-PCR		
Gene name	**Forward primer**	**Reverse primer**
MBP	5´GGCCGGACCCAAGATGAAAA 3´	5´CCCCAGCTAAACTGCTCAGG 3´
PLP1	5´TGCTGATGCCAGAATGTATGG 3´	5´GCAGATGGACAGAAGGTTGGA 3´
OLIG1	5´GTCATCCTGCCCTACTCAGC 3´	5´CAGCGTGGCTATCTTGGAGA 3´
CNP	5´CGCTCTACTTCGGCTGGTTC 3´	5´CCATCTTCTCCCTGGGCTCA 3´
GALC	5´CGAACTCTTCAAGGTGGTTGAT 3´	5´GCCTGCACCCATGTCACTATT 3´
GAPDH	5´CTGGTAAAGTGGATATTGTTGCCAT 3´	5´TGGAATCATATTGGAACATGTAAACC 3´
CSPG4	5´AGGACGAAGGAACCCTAGAGT 3´	5´CACAGGCACACTGTTGTGGA 3´
end.SOX10	5´GTTGACTGTTGCACCCACAC 3´	5´AGGTCCTGGGATAGAGGGTC 3´
end.OLIG2	5´GAGCTGGTCCAGTAGACATCG 3´	5´CACGCTCTCAGGGAAAGAAG 3´
FIBRONECTIN	5´CCACCCCCATAAGGCATAGG 3´	5´GTAGGGGTCAAAGCACGAGTCATC 3´
VIMENTIN	5´CCCTCACCTGTGAAGTGGAT 3´	5´TCCAGCAGCTTCCTGTAGGT 3´
THY1	5´ATCGCTCTCCTGCTAACAGTC 3´	5´ CTCGTACTGGATGGGTGAACT 3´
DKK3	5´ CTGGGAGCTAGAGCCTGATG 3´	5´ TCATACTCATCGGGGACCTC 3´

Supplemental Experimental Procedures

Plasmids and lentiviral preparation

Briefly, the cDNA sequences of human SON were inserted in a third-generation lentiviral vector in which they are co-expressed under a retroviral SFFV U3 promoter. The construct contains also an IRES-pac cassette allowing puromycin selection or IRES-RFP sequence enabling detection of the infected cells. The same backbone vector, without the SON sequences, was used as control (SF-puro).

For the lentiviral production 293T cells were co-transfected with the SF-SON-puro, SF-SON-RFP or SF-puro lentiviral vectors in addition to the packaging plasmids psPAX2 (Addgene #12260) and pMD2.G (Addgene #12259), using FuGENE HD (Promega). 72h post-transfection the collected supernatant was filtered with 0.45-µm PVDF membrane (Millipore) and viral particles were concentrated with ultracentrifugation. Viral pellets were resuspended in Dulbecco's Modified Eagle Medium high glucose (Sigma) and stored at −80 °C.

Cell Lines and culture

FibA, B and C were acquired from ATCC (PCS-201-010, CRL-2097, CCL-153, respectively). Fibroblasts derived from one individual with PLP1 643C>T mutation were acquired from Coriell Institute (ID:GM09546) while fibroblasts derived from three male individuals with PLP1 duplication were kindly provided by Prof. Odile Boespflug-Tanguy, LEUKOFRANCE Biobank, Biochemistry Department, Kremlin Bicetre Hospital, APHP, Paris. Fibroblasts from PMD patients were compared with sex and age matched controls as described in Table S2. For the DNA methylation assay neonatal fibroblasts were acquired from ATCC (PCS-201-010) and Coriell Institute (GM00041, GM08680), fibroblasts from middle aged donors were kindly provided by Jürgen Winkler or were generated at the UKM. Fibroblasts from old aged donors were provided from Jürgen Winkler (UKER-fG3G, UKERf-82A, UKERf-O3H). The study was approved by the local ethical committees in Münster, Erlangen, Milan and Paris (AZ 2018-040-f-S, AZ 259_17B and Banca INSpe, CPPAU788, CNIL1406552, AFSSAPS B90298-60).

Fibroblasts were cultured in fibroblast medium (FM): Dulbecco's Modified Eagle Medium high glucose (Sigma) containing 10% FBS (Gibco), 1% nonessential amino acids (NEAA) (Sigma), 1% GlutaMAX (Gibco), and 1% penicillin/streptomycin solution (Sigma). All cell lines were negative for HIV, HCV, HBV and mycoplasma contamination.

Flow cytometry analysis

Cells were enzymatically detached using accutase treatment for 5 min at 37 °C. Following washing with PBS cells were singularized by filtering through a 40-µm cell strainer (BD Falcon). Living cells were counted, blocked with cold PBS/0.5% BSA buffer and stained with mouse IgM anti–O4-APC antibody (Miltenyi Biotec) according to the manufacturer's protocol. Stained cells were washed, resuspended in PBS/0.5% BSA buffer and sorted using a FACS Aria cell sorter (BD Biosciences). Unstained cells were used to set the background fluorescence and human fibroblasts were used as negative control.

Migration assay

Purified O4 positive cells were plated (8.000cells/well) on a Poly-L-lysine (Sigma)/ hrLaminin (LN521, Biolaminin) coated 12 well plate in GIM. After 4h incubation at 37 °C an area of living cells was selected and monitored using the JulBr live cell analyzer. Photos were taken every 5min for 24h. The photos were merged to create a movie in ImageJ and the average cell velocity (µM/min) was measured.

Isolation of adult primary human oligodendrocytes

Brain tissue was obtained from adults undergoing surgical resections as treatment for non-tumor-related intractable epilepsy in accordance with the guidelines set by the Biomedical Ethics Unit of McGill University. As described (Cui et al., 2010) tissue specimens were enzymatically digested and placed on a linear 30% Percoll density gradient (Pharmacia Biotech, Piscataway, NJ). Microglia were separated and removed from the specimens by an initial adhesion step in which the total cell fraction was cultured for 24 hours in non-coated flasks. The floating cell fraction (referred to as primary human oligodendrocytes (pOL) was collected, resuspended in 250µl of RLT buffer (Quiagen) and shipped to Münster for RNA extraction.

RNA-seq analysis

To compare the global gene expression profile of dc-hiOLs with that of human fibroblasts and primary human oligodendrocytes three independent samples were analysed for each condition. Following total RNA extraction using the RNasy Mini Kit (Quiagen) and DNase (Quiagen) treatment the quality of the produced RNA was tested with Bioanalyzer analysis (Agilent). Samples with RIN value over 7 were used for RNA sequencing. mRNA enrichment (NEB) was followed by a directional library preparation (NEB) and single-end sequencing (Illumina NextSEq v 2.5) was performed at an average depth of 20.8 million reads. Transcript-level expression was quantified using Gencode v29 GRChr38 annotation and Salmon v0.9.1 (Patro et al., 2017). Gene-level expression was loaded into R using tximport v1.6.0. DESeq2 v1.18.1 (Love et al., 2014) was used to identify pairwise differential expression between conditions (dc-hiOLs vs fibroblasts and pOL vs fibroblasts) using a Wald test and an adjusted p-value < 0.01, as previously described (Jeong et al., 2017). We include a correction to account for donor effects when estimating differentially expressed genes between dc-hiOLs and fibroblasts by adding a donor term in the DEseq2 formula (design = ~ patient + condition). To assess gene ontology, disease and pathway annotation enrichment, hypergeometric tests adjusted for multiple testing using the Benjamini-Hochberg correction were performed with clusterProfiler v3.6.0 (FDR threshold < 0.01) (Yu et al., 2012). Only differentially expressed genes with associated Entrez IDs were used for this analysis.

Raw single-nucleus RNAseq read count data from Jäkel et al. 2019 (Jakel et al., 2019) was retrieved from GEO (accession number: GSE118257) and loaded into the R environment (version 3.6.0). Each single nucles was annotated according to the subclusters defined by Jäkel et al. and comprised 3530 oligodendrocytes (oligodendrocytes 1-6), 273 oligodendrocyte progenitor cells (OPCs), 81 immune oligodendroglia (ImOLG), 153 committed oligodendrocyte precursors (COPs), 1768 neurons (neurons 1-5), 454 astrocytes, 134 pericytes and 78 microglial cells. After read counts of each subcluster were averaged, the resulting data matrix was combined with read counts derived from our own RNA sequencing experiment. Quantile normalization was performed across the whole dataset. The resulting matrix was imported into DESeq2 (v1.26) using the DESeqDataSetFromMatrix() function. For visualisation, the expression dataset was transformed using variance stabilizing transformations (VST). For clustering analysis, 35 marker genes for OPCs, oligodendrocytes, neurons, astroglia, microglia and fibroblasts were selected. Samples were clustered using the Euclidean distance as the distance measure and complete linkage as the clustering method. The R script for the analysis is available on github (https://github.com/ctho1/compareRNAseq).

ATAC-seq analysis

Pair-end reads were filtered from adaptor contamination using Trim Galore v0.6 and aligned to the GRCh38 genome using Bowtie2 v2.3.4.3 (Langmead et al., 2009). Mitochondrial and duplicated reads were removed from downstream processing using Picard v.2.3. The nucleosome free fraction of the ATAC-seq fragments (insert sizes between 40-120bp) was used for visualization, clustering and peak calling purposes. Coverage tracks were calculated using deepTools bamCoverage v3.3.2 (Ramirez et al., 2016) with the following parameters: binSize 20, smoothLength 60, normalizeUsing BPM (Bins Per Million mapped reads).

Peak calling and differential accessibility: Broad peaks were called on each sample separately for initial characterization or on merged files of all conditions for differential accessibility tests using macs2 v2.2.6 (Feng et al., 2012) with parameters '-g hs --nomodel --qvalue 0.05 –broad'. Peaks were annotated using ChIPSeeker v1.2. Fragments mapping to peaks were summarized using featureCounts v1.6.5 (Liao et al., 2014) and differential accessibility was assessed using DESeq2 v1.24 (Love et al., 2014).

Motif enrichment: Short nucleosome free regions within differentially accessible peaks were called using NucleoATAC (Schep et al., 2015). HOMER v4.7 was used to scan for motifs found in the JASPAR database (Khan et al., 2018). Resulting motifs were plotted, clustered and aggregated using universalmotif v1.2.1 and R v3.6.1.

DNA methylation array analysis

To compare the methylation profile of fibroblasts and dc-hiOLs three independent samples per age-group were analyzed. Following total DNA extraction using the QIAamp DNA Mini Kit (Quiagen) all samples were analyzed using the MethylationEPIC BeadChip array (Illumina Inc., San Diego, CA). On-chip quality metrics of all samples were carefully controlled. Raw signal intensities from IDAT files were loaded into the R environment (version 3.6.0) using the minfi package (version 1.30). Quantile normalization was applied with the preprocessquantile function of the minfi package. The following filtering criteria were applied: removal of probes targeting the X and Y chromosomes, removal of probes containing a single nucleotide polymorphism (dbSNP132 Common) within

five base pairs of and including the targeted CpG site, and probes not mapping uniquely to the human reference genome (hg19) allowing for one mismatch. In total, 749.312 CpG sites were kept for analysis.
Unsupervised t-SNE analysis: Unsupervised t-Distributed Stochastic Neighbor Embedding (t-SNE) analysis was performed on the 5000 most variable methylation probes (standard deviation) across the whole dataset using the Rtsne package (version 0.15). The the following non-default parameter adjustments were used for t-SNE analysis: theta=0, max_iter=2000, perplexity=2. The results matrix was visualized with ggplot2 (version 3.2.1).

Focused analysis of *MBP*, *MAG* and *MOG* methylation levels**:** CpG probe annotation was performed with the getAnnotation function from minfi. Genomic coordinates of the human reference genome (hg19) from *MBP*, *MAG* and *MOG* were retrieved from NCBI (*MBP* chr18:74690789-74844774, *MAG* chr19:35782989-35804710, *MOG* chr6:29624758-29640149). Mean beta values for each gene were then compared between the fibroblasts and dciOL using the Wilcoxon test and results were visualized using ggplot2.

Differential methylation analyses: Differentially methylated probes between aged and neonatal samples were calculated using the limma package (3.40.6). A total of 57.106 CpG sites were differentially methylated. The top 1000 differentially methylated probes were then visualized using the pheatmap package (1.0.12). Differentially methylated regions between fibroblasts and dciOL samples were analyzed and visualized with DMRcate (2.0.7).

Compound treatment

For the promyelination compound screening the differentiation protocol was followed as described above until day 5. At day 5 the medium was changed to GIM supplemented with 1 µM SAG, 10 ng/mL PDGF, 200 µM AA and the tested compounds 1 µM miconazol (Sigma), 1 µM clemastine (Selleckchem) and 1 µM benztropine (Sigma). Medium change was performed every second day. At day 9 medium was switched to DM enriched by 0,5 µM SAG, 200 µM AA and 10 ng/mL PDGF. PDGF was replaced by 100 µM dbcAMP (Sigma) at day 12 and cells were analyzed with ICC at day 16. Compound treatment was continued until the last day. Negative controls were treated with the same volume of DMSO but no compound while positive controls were treated with 60 ng/mL T3.

For ER stress inhibition the typical transdifferentiation procedure was followed and cells were treated with 1µM GSK2656157 (Cayman Chemicals) or vehicle control from day 5 onwards.

Apoptosis assay

Magic Red Caspase3/7 Assay Kit (BIO RAD) was used for measurement of caspase activity. The assay is based on a cell-permeable and non-cytotoxic reagent which is cleaved in the presence of active caspases to produce a fluorescent product. The protocol was followed according to manufacturer´s instructions. Briefly, MR-(DEVD)2 substrate was added in the cell culture medium of bulk cells at day 13 for 45min. Following three washes with PBS cells were fixed with 4%PFA for 20min and immunostained for O4 as described above.

Supplemental Reference

CUI, Q. L., FRAGOSO, G., MIRON, V. E., DARLINGTON, P. J., MUSHYNSKI, W. E., ANTEL, J. & ALMAZAN, G. 2010. Response of Human Oligodendrocyte Progenitors to Growth Factors and Axon Signals. *J Neuropathol. Exp. Neurol*.

FENG, J., LIU, T., QIN, B., ZHANG, Y. & LIU, X. S. 2012. Identifying ChIP-seq enrichment using MACS. *Nat Protoc,* 7**,** 1728-40.

HEINZ, S., BENNER, C., SPANN, N., BERTOLINO, E., LIN, Y. C., LASLO, P., CHENG, J. X., MURRE, C., SINGH, H. & GLASS, C. K. 2010. Simple combinations of lineage-determining transcription factors prime cis-regulatory elements required for macrophage and B cell identities. *Mol Cell,* 38**,** 576-89.

JAKEL, S., AGIRRE, E., MENDANHA FALCAO, A., VAN BRUGGEN, D., LEE, K. W., KNUESEL, I., MALHOTRA, D., FFRENCH-CONSTANT, C., WILLIAMS, A. & CASTELO-BRANCO, G. 2019. Altered human oligodendrocyte heterogeneity in multiple sclerosis. *Nature,* 566**,** 543-547.

JEONG, H. W., HERNANDEZ-RODRIGUEZ, B., KIM, J., KIM, K. P., ENRIQUEZ-GASCA, R., YOON, J., ADAMS, S., SCHOLER, H. R., VAQUERIZAS, J. M. & ADAMS, R. H. 2017. Transcriptional regulation of endothelial cell behavior during sprouting angiogenesis. *Nat Commun,* 8**,** 726.

KHAN, A., FORNES, O., STIGLIANI, A., GHEORGHE, M., CASTRO-MONDRAGON, J. A., VAN DER LEE, R., BESSY, A., CHENEBY, J., KULKARNI, S. R., TAN, G., BARANASIC, D., ARENILLAS, D. J., SANDELIN, A., VANDEPOELE, K., LENHARD, B., BALLESTER, B., WASSERMAN, W. W., PARCY, F. & MATHELIER, A. 2018. JASPAR 2018: update of the open-access database of transcription factor binding profiles and its web framework. *Nucleic Acids Res,* 46**,** D260-D266.

LANGMEAD, B., TRAPNELL, C., POP, M. & SALZBERG, S. L. 2009. Ultrafast and memory-efficient alignment of short DNA sequences to the human genome. *Genome Biol,* 10**,** R25.

LIAO, Y., SMYTH, G. K. & SHI, W. 2014. featureCounts: an efficient general purpose program for assigning sequence reads to genomic features. *Bioinformatics,* 30**,** 923-30.

LOVE, M. I., HUBER, W. & ANDERS, S. 2014. Moderated estimation of fold change and dispersion for RNA-seq data with DESeq2. *Genome Biol,* 15**,** 550.

PATRO, R., DUGGAL, G., LOVE, M. I., IRIZARRY, R. A. & KINGSFORD, C. 2017. Salmon provides fast and bias-aware quantification of transcript expression. *Nat Methods,* 14**,** 417-419.

RAMIREZ, F., RYAN, D. P., GRUNING, B., BHARDWAJ, V., KILPERT, F., RICHTER, A. S., HEYNE, S., DUNDAR, F. & MANKE, T. 2016. deepTools2: a next generation web server for deep-sequencing data analysis. *Nucleic Acids Res,* 44**,** W160-5.

SCHEP, A. N., BUENROSTRO, J. D., DENNY, S. K., SCHWARTZ, K., SHERLOCK, G. & GREENLEAF, W. J. 2015. Structured nucleosome fingerprints enable high-resolution mapping of chromatin architecture within regulatory regions. *Genome Res,* 25**,** 1757-70.

YU, G., WANG, L. G., HAN, Y. & HE, Q. Y. 2012. clusterProfiler: an R package for comparing biological themes among gene clusters. *OMICS,* 16**,** 284-7.